A multi–Lorentzian timing study of the atoll sources 4U 0614+09 and 4U 1728–34

Steve van Straaten[1], Michiel van der Klis[1], Tiziana di Salvo[1], Tomaso Belloni[2], Dimitrios Psaltis[3]

ABSTRACT

We present the results of a multi–Lorentzian fit to the power spectra of two kilohertz QPO sources; 4U 0614+09 and 4U 1728–34. This work was triggered by recent results of a similar fit to the black–hole candidates (BHCs) GX 339–4 and Cyg X–1 by Nowak in 2000. We find that one to six Lorentzians are needed to fit the power spectra of our two sources. The use of exactly the same fit function reveals that the timing behaviour of 4U 0614+09 and 4U 1728–34 is almost identical at luminosities which are about a factor 5 different. As the characteristic frequency of the Lorentzians we use the frequency, $\nu_{\rm max}$, at which each component contributes most of its variance per log frequency as proposed by Belloni, Psaltis & van der Klis in 2001. When using $\nu_{\rm max}$ instead of the centroid frequency of the Lorentzian, the recently discovered hectohertz Lorentzian is practically constant in frequency. We use our results to test the suggestions by, respectively, Psaltis Belloni and van der Klis in 1999 and Nowak in 2000 that the two Lorentzians describing the high–frequency end of the broad-band noise in BHCs in the low state can be identified with the kilohertz QPOs in the neutron star low mass X–ray binaries. The prediction for the neutron star sources is that if the two kilohertz QPOs are present, then these two high–frequency Lorentzians should be absent from the broad–band noise. We find, that when the two kilohertz QPOs are clearly present, the low–frequency part of the power spectrum is too complicated to draw immediate conclusions from the nature of the components detected in any one power spectrum. However, the relations we observe between the characteristic frequencies of the kilohertz QPOs and the band–limited noise, when compared to the corresponding relations in BHCs, hint towards the identification of the second–highest frequency Lorentzian in the BHCs with the lower kilohertz QPO. They do not confirm the identification of the highest–frequency Lorentzian with the upper kilohertz QPO.

Subject headings: accretion, accretion disks — binaries: close — stars: individual (4U 1728–34, 4U 0614+09) — stars: neutron stars: oscillations— X–rays: stars

1. Introduction

Low mass X-ray binaries (LMXBs) can be divided into black–hole candidates (BHCs) and neutron–star LMXBs. The accretion process in these LMXBs can be studied through the timing properties of the associated X-ray emission (see for an overview van der Klis 2000). The Fourier power spectra of the neutron–star LMXBs contain several timing features; a power–law red noise component in the lowest frequency range of the spectrum ($\nu < 1$ Hz) called very low frequency noise (VLFN), a band–limited noise component (BLN) which is in most cases flat at low frequency and steepens to an approximate power–law with an index of about 1 at higher frequency and several quasi–periodic oscillations (QPOs) at

[1]Astronomical Institute, "Anton Pannekoek", University of Amsterdam, and Center for High Energy Astrophysics, Kruislaan 403, 1098 SJ Amsterdam, The Netherlands.

[2]Osservatorio Astronomico di Brera, Via E. Bianchi 46, I-23807 Merate (LC), Italy.

[3]Center For Space Research, Massachusetts Institute of Technology, Cambridge, MA 02139, USA

low ($\nu \lesssim 100$ Hz) and high frequencies. The high frequency QPOs, at frequencies from a few hundred Hz to more than 1000 Hz are called kilohertz QPOs. The correlation between the timing features at low frequency and the spectral properties led to a precise classification of the neutron star systems as Z or atoll sources (Hasinger & van der Klis 1989). Note, that the component that we call BLN has been previously called "high–frequency noise" in atoll sources; this is presumably the same phenomenon that is called "low–frequency noise" in Z sources (cf. van der Klis 1995). The timing features of the BHCs include among others a band–limited noise component, a bump between 1 and 10 Hz and several QPOs. For the low–frequency ($\nu \lesssim 100$ Hz) part of the power spectrum links between BHCs in the low state and neutron–star LMXBs were suggested (e.g., van der Klis 1994a,b), in particular concerning the band–limited noise and some of the QPOs.

The improved sensitivity and the discovery of several new timing features with the Rossi X–ray Timing Explorer (RXTE) has opened up new possibilities for connecting the timing properties of the neutron–star LMXBs and the BHCs. In the atoll source 4U 0614+09 van Straaten et al. (2000, hereafter vS00) found that the relation between power density and break frequency of the band–limited noise was similar to that established for BHCs in the low state. Wijnands & van der Klis (1999, hereafter WK99) showed that the break frequency of the band–limited noise and the centroid frequency of a low–frequency QPO follow the same correlation for both the neutron–star LMXBs and the BHCs. Psaltis, Belloni & van der Klis (1999, hereafter PBK99) made a systematic study of QPOs and broad–band noise components of the neutron–star LMXBs and the BHCs. They suggested the identification of two features by plotting their frequencies versus each other. The BHCs' high–frequency bump between 1 and 10 Hz was tentatively identified with the lower kilohertz QPO in the Z and atoll sources and the BHCs' low–frequency QPO with the horizontal branch oscillations/low–frequency QPO in the Z/atoll sources.

Recently, Nowak (2000) described the power spectra of the BHCs GX 339–4 and Cyg X–1 with a fit function consisting of four Lorentzian components and suggested the identification of the two highest frequency Lorentzians, which together describe the high–frequency end of the broad–band noise, with the two kilohertz QPOs. The Lorentzian that is used to fit the low–frequency end of the broad–band noise has a centroid frequency fixed to zero. In the picture of Nowak (2000) for the BHCs the first Lorentzian corresponds to the broken power law of WK99, the second Lorentzian to the low–frequency QPO of WK99 and PBK99 and the third Lorentzian to the high–frequency bump between 1 and 10 Hz of PBK99. This work forms the original motivation for the current paper. Also triggered by Nowak (2000), Belloni, Psaltis & van der Klis (2001, hereafter BPK01) describe a paradigm for fitting the power spectra of low–luminosity bursters and BHCs in their low/hard state. They describe the power spectra of these sources with a fit function consisting of four Lorentzian components of which in practice three are zero–centered. The suggestion of Nowak (2000) might be tested by comparing his black hole results with neutron star sources, where both kilohertz QPOs can be clearly identified and strong broad–band noise is simultaneously present: the prediction for the neutron star sources is that if the two kilohertz QPOs are present the two high–frequency Lorentzians should be absent from the broad–band noise. In this work we test the multi–Lorentzian fit function of Nowak (2000) and BPK01 on two of the atoll sources, namely 4U 1728–34 and 4U 0614+09. The timing properties at low and high frequencies of 4U 1728–34 and 4U 0614+09 have previously been studied in connection with the properties of the X–ray energy spectrum by vS00 for 4U 0614+09 and Di Salvo et al. (2001, hereafter DS01) for 4U 1728–34. In these papers a broken power–law was used to fit the band–limited noise component, although the alternative of using a Lorentzian was also considered. The X–ray energy spectrum was studied by using color diagrams, where a color is the ratio of two X–ray count rates in different energy bands. Strong correlations were found between the frequencies of several components and properties of the X–ray energy spectrum. DS01 and vS00 also showed that both 4U 1728–34 and 4U 0614+09 followed the WK99 and PBK99 relations described above.

We find that instead of four Lorentzians one to six Lorentzians are needed to fit the power spectra

of 4U 1728–34 and 4U 0614+09. We describe these different Lorentzian components in §3. In §4 we compare our results with those of Nowak (2000) and BPK01.

2. Observations and Data Analysis

In this work we analyse data from RXTE's proportional–counter array (PCA; for instrument information see Zhang et al. 1993) of the neutron–star LMXBs 4U 1728–34 and 4U 0614+09. For 4U 1728–34 we used the Fourier power spectra 1 to 19 obtained by and described in DS01. The power spectra were constructed by dividing the PCA light curve into segments of 256 s and then binning the data in time before Fourier transforming such that the Nyquist frequency is always 2048 Hz; the normalization of Leahy et al. (1983) was used. Power spectra were combined based on the position in the color diagram, which is thought to be an indicator of mass accretion rate. The resulting power spectra were then converted to squared fractional rms. The Poisson noise estimated between 1200 and 2048 Hz (where neither noise nor QPOs are known to be present) was subtracted before fitting the power spectra.

For 4U 0614+09 we use a large data set previously studied by vS00 plus in addition recent observations performed between 2000 September 1 and 4 and 2001 May 24 and 28. In the September 2000 observations the source was at levels corresponding to the lowest mass accretion rate (as inferred from colors and power–spectral properties) observed by vS00. In the May 2001 observations the inferred mass accretion rate was at an even lower level. Starting May 12, 2000, the propane layer on PCU0, which functions as an anti–coincidence shield for charged particles, was lost. This leads to a contamination of the data from electrons trapped in the Earth's magnetosphere or from solar flare activity. For the September 2000 and May 2001 observations we therefore exclude all data with ELECTRON2 > 0.09, where ELECTRON2 is the measured coincidence of events between the PCU propane layer and either of the two anodes in the first layer of PCU2, the only detector that was switched on in all the observations. The ELECTRON2 screening led to a loss of about 12% of the data.

In vS00 the 4U 0614+09 data were split into near–continuous time intervals of approximately 2500 s which were called observations. For the present work, to improve statistics, we constructed representative intervals by adding up several observations that showed very similar power spectra in vS00. As all characteristic frequencies in the power spectra are correlated with each other and with the position of the source in the hardness–intensity diagram (parametrized in vS00 by a variable $S_{\rm a}$) we can select the data on one of these frequencies. The only power spectral feature that is present in all observations is the high–frequency noise. However, at a $\nu_{\rm break}$ (the break frequency of the band–limited noise, see for a definition vS00) of about 25 Hz and higher the correlation with the other frequencies and with the position in hardness–intensity diagram breaks down (see figures 3 and 6 in vS00). Therefore, for a $\nu_{\rm break}$ well below 25 Hz we used $\nu_{\rm break}$ to select the data and for a $\nu_{\rm break}$ of about 25 Hz and higher we used the centroid frequencies of the kilohertz QPOs. To represent the highest mass accretion rate in 4U 0614+09 (where the kilohertz QPOs are mostly absent) we add up the two observations at $S_{\rm a} = 2.59$ and $S_{\rm a} = 2.64$ in vS00. As in the case of 4U 1728–34, we number the intervals (1–9) in order of an increasing inferred mass accretion rate. We note that we could have selected the data based on $S_{\rm a}$ value as was done for 4U 1728–34 (see above), but because of the scatter in the correlation of $S_{\rm a}$ with the frequencies of the power spectral features (see figures 3 and 4 in vS00), in 4U 0614+09 this leads to an artificial broadening of the power spectral features and in the case of the kilohertz QPOs sometimes even to double peaks.

For each interval of 4U 0614+09 we constructed a power spectrum in the same fashion as for 4U 1728–34 (see above), but with a Nyquist frequency of 4096 Hz. An interval contains between 53 and 382 power spectra. We subtracted the Poisson noise estimated between 2000 and 4000 Hz (as, different from 4U 1728–34, QPOs are known to be present between 1200 and 1400 Hz) before fitting the power spectra.

We fitted the power spectra with a sum of Lorentzian components. One to six Lorentzian components were needed for a good fit. We only include those Lorentzians in the fit whose significance based on the error in the power integrated from 0 to ∞ is above 3.0 σ. In addition to the

Lorentzians a power–law component is used to fit the so called very low–frequency noise (VLFN). For the intervals where the kilohertz QPOs have sufficiently high frequencies not to interfere with the low–frequency features and vice versa, we fit the kilohertz QPOs between 500 and 2048 Hz and then fix the kilohertz QPO parameters when we fit the whole power spectra, similar to what was done in DS01. This is for computational reasons only; the results are the same as those obtained with all parameters free.

We plot the power spectra and the fit functions in the power times frequency representation (e.g. Belloni et al. 1997, Nowak 2000), where the power spectral density is multiplied with its Fourier frequency. For a fit function consisting of many Lorentzians this representation helps to visualize a characteristic frequency corresponding to each Lorentzian component (BPK01) namely, the frequency where each component contributes most of its variance per logarithmic frequency interval. This characteristic frequency, is not equal to the centroid frequency, ν_0, of the Lorentzian but to $\nu_{\rm max} = \sqrt{\nu_0^2 + \Delta^2}$, where Δ is the HWHM of the Lorentzian. In this work we therefore use $\nu_{\rm max}$ as characteristic frequency for broad features. For narrow features the characteristic frequency is nearly the same as ν_0. All power spectral features that we find in 4U 0614+09 and 4U 1728–34 become broader towards lower interval number (see §3). Several features can be classified as QPOs at higher characteristic frequencies but evolve into broad bumps as their frequencies become lower. Therefore, to be consistent we use $\nu_{\rm max}$ for all features. The actual Lorentzian functions fitted were of the form:

$$P(\nu;\nu_{\rm max},Q,r) = \frac{r^2\Delta}{(\frac{\pi}{2} + \arctan 2Q)(\Delta^2 + (\nu - 2\Delta Q)^2)}$$

where $\Delta = \nu_{\rm max}/\sqrt{1+4Q^2}$, and r (the fractional rms integrated from 0 to ∞), Q (the quality factor, defined as $\nu_0/2\Delta$) and $\nu_{\rm max}$ were the independent fit parameters.

3. Results

The two sources 4U 1728–34 and 4U 0614+09 yielded remarkably similar results. One to six Lorentzian components were needed for a good fit. In addition to these Lorentzians, intervals 14–19 of 4U 1728–34 and 8 and 9 of 4U 0614+09 needed a power–law component to fit the very low–frequency noise (VLFN). We show power spectra and fit functions in Figure 1 for 4U 1728–34 and in Figure 2 for 4U 0614+09. The values of $\nu_{\rm max}$ for all Lorentzian components are listed in Table 1, the values of Q are listed in Table 2 and the values of the integrated fractional rms (over the full PCA energy band) are listed in Table 3. The quoted errors in $\nu_{\rm max}$, Q and r use $\Delta\chi^2 = 1.0$.

The χ^2/dof values of the fits are listed in Table 4. For comparison the χ^2/dof values of a broken power–law fit (for a description see DS01) to the same intervals are also included. There seems to be a clear statistical preference for the multi–Lorentzian function. For rather similar numbers of degrees of freedom (between 131 and 145, and usually higher in the multi–Lorentzian than in the broken power–law fit) the χ^2 values of the multi–Lorentzian fits are more than 10 lower than of the broken power–law fits in 15 out of 28 cases, whereas the inverse is true in only 4 of the 28 cases. The fits are generally better for 4U 0614+09 (all with a χ^2/dof below 1.9) than for 4U 1728–34 (χ^2/dof below 4.1); this could be due to the different methods used to select the data (see §2).

Allmost all fitted power–spectral features (described below) were already identified in DS01 and vS00. In DS01 and vS00 the BLN component is described with a broken power law, whereas we use a zero-centered Lorentzian. As in DS01 and vS00 we use Lorentzians to describe two low–frequency QPOs (when present), a broad high–frequency feature ($\sim$ 100 Hz) and the two kilohertz QPOs. We do not describe the behaviour of the VLFN component in this work; for a discussion of this component in 4U 1728–34 and 4U 0614+09 see respectively DS01 and vS00. In the current work, it only affects the power spectra below 0.1–1 Hz.

To confirm the identification of the components, we have plotted the $\nu_{\rm max}$ of the Lorentzians versus the $\nu_{\rm max}$ of the Lorentzian identified as the upper kilohertz QPO ($\nu_{\rm upperkHz}$) in Figure 3. Intervals 18 and 19 of 4U 1728–34 are not included in this plot as these intervals only showed one Lorentzian. The grey symbols mark the 4U 1728–34 points, the black symbols the 4U 0614+09 points. In Figure 3 five correlations are present, of which the top three can be unambiguously identified with the Lorentzians described in §3.2–3.4. For the other two correlations the identification is more compli-

cated; see §3.1. The points from interval 1 of 4U 0614+09 (from recent observations in May 2001) are circled. The Lorentzian at 233 Hz of this interval can be identified based on frequency, Q value or fractional rms as either the upper kilohertz QPO or the hectohertz Lorentzian. In Tables 1, 2 and 3 we list this Lorentzian as the upper kilohertz QPO. In Figure 3 and in all further figures we will use the parameters of this Lorentzian both for the upper kilohertz QPO and for the hectohertz Lorentzian. These points will be circled.

The two sources show a remarkable similarity in their behaviour. This similarity is also shown in the behaviour of the Q values (Table 2) and the fractional rms's of the different components (Table 3), although the fractional rms in 4U 0614+09 is generally higher by about a factor of 1.3 to 2 than that in 4U 1728–34. Note that the hydrogen column density, $N_{\rm H}$, is about a factor 10 higher for 4U 1728–34 (e.g. Schultz 1999). This leads to the absorbtion of more low–energy photons for 4U 1728–34 than for 4U 0614+09 and could increase the factor as most power spectral features are stronger at higher energies. In Figures 4 and 5 we plot the fractional rms and the Q value of the hectohertz Lorentzian, the lower and upper kilohertz QPOs (see below for a description of these components) versus $\nu_{\rm upperkHz}$.

3.1. The band–limited noise

The zero–centered Lorentzian which is used to fit the band–limited noise (BLN), is present in most of the intervals (except interval 9 of 4U 0614+09). As noted in §1, previously the BLN in the atoll sources was referred to as HFN (high frequency noise) in the literature, but as it has the lowest characteristic frequency of all components that name seems no longer appropriate. The characteristic frequency of this component ($\nu_{\rm BLNZERO}$), increases with interval number. This increase is halted at interval 13 for 4U 1728–34 and interval 5 for 4U 0614+09. Here an additional, non zero–centered Lorentzian component had to be included in the fit to the BLN. As previously noted by DS01, the characteristic frequency of this new component, $\nu_{\rm BLNQPO}$, continues to follow the relations between the $\nu_{\rm BLNZERO}$ and the characteristic frequencies of the other components (see Fig. 3) as well as the relation with interval number. We shall refer to this Lorentzian as the BLN QPO. The BLN QPO is generally broader at lower frequencies (see Tables 1 and 2) except for interval 18 and 19 of 4U 1728–34 and 9 of 4U 0614+09 for which the identification as BLN QPO is ambiguous (see below). Note that in the broken power law description, the BLN QPO is usually not statistically required in 4U 0614+09, whereas it is in 4U 1728–34 (DS01).

In Figure 6 we plot the fractional rms of the BLN versus $\nu_{\rm upperkHz}$. In the top panel we plot the fractional rms of the zero–centered Lorentzian. In the middle panel we plot the fractional rms of the BLN QPO when it is present, and the fractional rms of the zero–centered Lorentzian when it is not. In the bottom panel finally we plot the fractional rms of the zero–centered Lorentzian and the BLN QPO summed together. In the top two panels the relation tends to jump when the BLN QPO appears, where this jump does not occur in the bottom plot. The relation is also smoother in the bottom plot. This behaviour hints at the zero–centered Lorentzian and the BLN QPO being two components that together fit one feature.

In intervals 18 and 19 of 4U 1728–34 and 9 of 4U 0614+09 there is only one Lorentzian present. Based on the relations of characteristic frequency, Q and rms fractional amplitude with interval number, this Lorentzian can be identified as either one of the two BLN Lorentzians. As fitting this Lorentzian with a zero–centered Lorentzian provides bad fits, we have listed it as the BLN QPO in Tables 1 and 2, but this identification is uncertain. Contrary to all other components, the characteristic frequency of this component decreases with interval number (see Tables 1 and 2).

3.2. The low–frequency Lorentzian

The second Lorentzian at low frequencies (which we shall refer to as the low–frequency Lorentzian) was present in intervals 1–12 for 4U 1728–34 and 1–6 for 4U 0614+09 (see Figures 1 and 2). The characteristic frequency of this component, $\nu_{\rm LF}$, also increases with interval number (see Table 1). In 4U 1728–34 $\nu_{\rm LF}$ ranges from 11.5–46.7 Hz, in 4U 0614+09 from 2.0–44.6 Hz. The low–frequency Lorentzian is too broad to be classified as a QPO ($Q < 2$) at low frequencies ($\nu_{\rm LF} < 25$ Hz; see Tables 1 and 2) and Q only exceeds 2 at higher frequencies. Note that the low–frequency Lorentzian might be present in in-

terval 6 of 4U 0614+09 ($\nu_{\rm LF} = 60.5^{+1.6}_{-2.2}$ Hz); as the significance based on the error in the integrated power is only 2.4 σ we have not included this Lorentzian in the fit.

3.3. The hectohertz Lorentzian

The fourth component, which we shall refer to as the hectohertz Lorentzian, is fitted with a Lorentzian with a characteristic frequency of the order of 100 Hz. The hectohertz Lorentzian is only absent in intervals 18 and 19 of 4U 1728–34, at the highest inferred mass accretion rate. The Lorentzian at 233 Hz in interval 1 of 4U 0614+09, at the lowest inferred mass accretion rate, can be identified as either the hectohertz Lorentzian or the upper kilohertz QPO. The hectohertz Lorentzian is broad at low interval numbers and becomes narrower at high interval numbers (see Table 2). This is a good example of how the characteristic frequency $\nu_{\rm max}$ of a Lorentzian is determined by ν_0 and Δ. In Figure 7 we plot $\nu_{\rm max}$, ν_0 and Δ versus the centroid frequency of the upper kilohertz QPO. As ν_0 increases, Δ falls such that $\nu_{\rm max}$ is nearly constant.

3.4. The kilohertz QPOs

The fifth and sixth Lorentzians were used to fit the pair of kilohertz QPOs. This pair is present in intervals 10–17 for 4U 1728–34 and 6–8 for 4U 0614+09. In interval 1 of 4U 0614+09 there is a Lorentzian present at $\sim$ 20 Hz. Based on its frequency this Lorentzian can be tentatively identified with the relation which PBK99 associate with the lower kilohertz QPO. However, this Lorentzian is much broader and stronger than any of the "normal" lower kilohertz QPOs in 4U 0614+09 and 4U 1728–34 (see Figures 4 and 5); its broad shape is similar to the corresponding feature seen at similar frequencies in the low–luminosity bursters (BPK01). In the other intervals (except 18 and 19 for 4U 1728–34) there is only one kilohertz QPO present, which can be identified as the upper kilohertz QPO based on the correlations of its frequency with the frequency of the other features (see Fig. 3) or interval number (see DS01). The Lorentzian at 233 Hz in interval 1 of 4U 0614+09 can be identified as either the hectohertz Lorentzian or the upper kilohertz QPO. Both kilohertz QPOs are broader at lower frequencies (see Tables 1 and 2). At frequencies below $\sim$ 550 Hz the upper kilohertz QPO becomes too broad to be classified as a real QPO ($Q < 2$).

4. Comparison with other sources

A way to compare the results of our multi–Lorentzian fit to the two atoll sources with previous fits of this function to other neutron–star LMXBs and BHCs (Shirey 1998, Nowak 2000, BPK01) is to plot the characteristic frequencies of the different Lorentzians components versus the frequency of one Lorentzian component which has already been identified for all these sources. There are three obvious candidates to plot everything against that have already been identified by WK99 and PBK99 (see the introduction): the band–limited noise component, the low–frequency Lorentzian and the lower kilohertz QPO. Here we choose to present the results of comparing to the band–limited noise component. If we use the characteristic frequency of the low–frequency Lorentzian instead, our conclusions do not change. If we use the characteristic frequency of the lower kilohertz QPO our points fall on the relations shown in BPK01 (see Figure 8); any differences between our conclusions and those of BPK01 are discussed below.

The large advantage of using the band–limited noise component is that in our data this component is present in all spectra, whereas the lower kilohertz QPO is only present in 11 (perhaps 12, see §3.4) and the low–frequency Lorentzian in 18 out of the 28 power spectra. Also in the other sources the band–limited noise component can almost always be clearly identified, where for the other peaks there can be ambiguity about which peak is which (see, e.g., Homan et al. 2001). A disadvantage of using the band–limited noise component is that in both 4U 1728–34 and 4U 0614+09 at a certain point the BLN QPO "takes over" from the zero–centered Lorentzian (see §3.1). So, just plotting the characteristic frequencies of the different Lorentzian components versus $\nu_{\rm BLNZERO}$ leads to a confusing picture where the correlations break down, i.e. at the intervals where both the zero–centered Lorentzian and the BLN QPO are present. This can be resolved by using $\nu_{\rm BLNQPO}$ as the characteristic frequency of the the band–limited noise if the BLN QPO is present, and $\nu_{\rm BLNZERO}$ otherwise. We call the thus defined

characteristic frequency of the band–limited noise $\nu_{\rm band}$. We caution that due to the extensive data sets available for our two sources we are able to keep track of $\nu_{\rm band}$ through the transformation from zero–centered Lorentzian to BLN QPO. With less data, confusion is likely. The correlation of $\nu_{\rm band}$ with the other frequencies breaks down at interval 9 of 4U 0614+09 (cf. §3.1). However, as this is only one very extreme point this is not a real problem for our present purpose. We have excluded intervals 18 and 19 of 4U 1728–34 from the correlations, as for these intervals only one component, the BLN QPO, is present. But note that in these intervals also there is evidence of a break down in the correlations with $\nu_{\rm band}$ (§3.1).

In Figure 9 we compare our results with those of Nowak (2000; GX 339–4, Cyg X–1) and BPK01 (1E 1724–3045, GS 1826–24, SLX 1735–269, XTE J1118+480) by plotting all characteristic frequencies versus $\nu_{\rm band}$. We have also included the results for Cir X–1 from Shirey (1998) that were also used in PBK99. That author also used a zero–centered Lorentzian to fit the broad–band noise, and fitted two peaked features with Lorentzians. The only difference with Nowak (2000) and BPK01 is that the high–frequency tail in Shirey (1998) was fitted with a power law, whereas Nowak (2000) and BPK01 use an additional Lorentzian. The grey symbols in Fig. 9 represent the results from Shirey (1998), Nowak (2000) and BPK01, the black symbols our results on 4U 1728–34 and 4U 0614+09. For clarity Figure 9 is split up in three panels. In the bottom panel we plot the characteristic frequency of the low–frequency Lorentzian ($\nu_{\rm LF}$), versus $\nu_{\rm band}$ (the WK99 relation). In this plot we have included the points from WK99 without the 4U 1728–34 and 4U 0614+09 points. However, note that WK99 use a broken power–law instead of a zero–centered Lorentzian to fit the band–limited noise. This will lead to systematic deviations in characteristic frequency (see BPK01). Also note that for both 1E 1724–3045 and GS 1826–24 there are usually two low frequency peaks present (see BPK01); a narrow peak and a broad component at a slightly higher frequency. If both these peaks are present we use the $\nu_{\rm max}$ of the broad peak to compare with 4U 1728–34 and 4U 0614+09 based on the strong similarities of the broad peak with the low frequency Lorentzian in these sources (see also Figure 10).

Most of our results on 4U 1728–34 and 4U 0614+09 coincide with the WK99 data. A few points lie slightly below the WK99 relation just as the points of GX 339–4, Cyg X–1 of Nowak (2000) and 1E 1724–3045, GS 1826–24 and SLX 1735–269 of BPK01. This may be due to the systematic frequency deviations between a zero–centered–Lorentzian and a broken power–law (see BPK01). The XTE J1118+480 points of BPK01 and the Cir X–1 points of Shirey (1998) are well below the WK99 relation but may line up with each other. Note that the QPO in Cir X–1 was previously identified as $\nu_{\rm LF}$ with the PBK99 relation (see PBK99).

In the middle and top panels we plot the characteristic frequencies of the hectohertz Lorentzian and both kilohertz QPOs versus $\nu_{\rm band}$ for 4U 1728–34 and 4U 0614+09. We have fitted the correlations of the characteristic frequencies of the hectohertz Lorentzian and the upper kilohertz QPO to $\nu_{\rm band}$ with power–laws in order to extrapolate these correlations to lower frequencies (dashed lines in Fig. 9). For the lower kilohertz QPO the range in $\nu_{\rm band}$ from these two sources alone is too small to draw strong conclusions from the extrapolation. For these fits we excluded interval 9 of 4U 0614+09 where the correlations between $\nu_{\rm band}$ and the frequencies of the other Lorentzians break down (see Fig. 3). We also exclude interval 1 of 4U 0614+09 from the fit (although these points are shown in the Figure) as for this interval the identification of the hectohertz Lorentzian and the lower and upper kilohertz QPO are uncertain (see §3). We use these power–law fits only to get an indication for what the characteristic frequencies for the hectohertz Lorentzian and the upper kilohertz QPO would be expected to be at low frequencies. The difference between the two panels is that in the middle panel we compare with the characteristic frequency of the Lorentzian (ν_ℓ in BPK01) that PBK99 (for the points from Shirey 1998), Nowak (2000) and BPK01 identify with the lower kilohertz QPO and in the top panel with the Lorentzian (ν_u in BPK01) that Nowak (2000) and BPK01 identify with the upper kilohertz QPO. We find that also when plotting versus $\nu_{\rm band}$ the relation between ν_ℓ and $\nu_{\rm band}$ (middle frame) is similar to the relation of the lower kilohertz QPO with $\nu_{\rm band}$. Also the $\sim$ 20 Hz Lorentzian of interval 1

of 4U 0614+09 falls fairly close to the relation between ν_ℓ and $\nu_{\rm band}$. However, more work needs to be done to connect both relations.

Concerning the top panel, Nowak (2000) and BPK01 found that the BHC points (GX 339–4, Cyg X–1 and XTE J1118+480) as well as the SLX 1735–269 point followed the extension to low frequencies of the "lower versus upper kilohertz QPO frequency" of PBK99. The points of 1E 1724–3045 and GS 1826–24 were above the relation. We find that the BHC points (GX 339–4, Cyg X–1 and XTE J1118+480) as well as the single point from SLX 1735–269 lie well below the extrapolated relation of $\nu_{\rm band}$ with the characteristic frequency of the upper kilohertz QPO; the points might be consistent with the extrapolation of the lower kilohertz QPO relation. We can therefore not identify the highest frequency Lorentzian in these sources with the upper kilohertz QPO based on this relation. Note again that the identification of $\nu_{\rm band}$ might be wrong in sources for which only litle data has been analyzed (see above). The points of GS 1826–24 are well above the relation and only the points of 1E 1724–3045 fall in the right range. However, the 1E 1724–3045 points also fall in the right range to be identified with the hectohertz Lorentzian. The same conclusion can be drawn for the 233 Hz Lorentzian of interval 1 of 4U 0614+09.

Interval 1 of 4U 0614+09 shows a $\nu_{\rm band}$ similar to that of the Cyg X–1 observation from Nowak (2000) and to that of observations of the low luminosity bursters 1E 1724–3045 and GS 1826–24 from BPK01. In Figure 10 we plot the power spectra of 4U 0614+09, 1E 1724–3045 and Cyg X–1 that have a $\nu_{\rm band}$ of about 0.3 Hz. For 1E 1724–3045 we use the same data that made up interval E of BPK01 and for Cyg X–1 we use the RXTE observations on 1996 October 22, the same as used by Nowak (2000). We constructed the power spectra in the same fashion as for 4U 1728–34 and 4U 0614+09 (see §2). The power spectra of 4U 0614+09 and 1E 1724–3045 are almost identical at both low and high frequencies. The power spectrum of Cyg X–1 is only similar to those of the neutron stars at low frequencies. The two high frequency peaks are both weaker relative to the low frequency peaks and about a factor of 4 lower in characteristic frequency than those in 4U 0614+09 and 1E 1724–3045. An explanation for this might be that the characteristic frequencies of the high frequency peaks in the spectrum scale with the mass of the central object and that the low frequency peaks are independent of this mass.

5. Discussion

5.1. Comparison between 4U 1728–34 and 4U 0614+09

The use of exactly the same fit function for both 4U 1728–34 and 4U 0614+09 shows the similar timing behaviour of these two atoll sources (see §3). Especially the frequencies and the Q values are almost identical. This similarity is quite remarkable, as the X–ray luminosity is about a factor 5 larger for 4U 1728–34 (Ford et al. 2000). The fractional rms in 4U 1728–34 is systematically lower than that in 4U 0614+09, which may be related to its higher luminosity. Note that the data are inconsistent with a model in which the kilohertz QPO amplitudes are the same and the higher luminosity of 4U 1728–34 is caused by an additional source of X–rays unrelated to the kilohertz QPOs; then the rms values in 4U 1728–34 would be expected to be a factor of 5 lower, while they are only lower by about a factor of 1.3 to 2. Another stunning difference between 4U 1728–34 and 4U 0614+09 is that in the whole RXTE data set on 4U 0614+09 obtained until now ($\sim$ 900 ks) no type I X–ray bursts have been observed, whereas 4U 1728–34 is a well known burster that shows type I X–ray bursts in all parts of the color–color diagram (van Straaten et al. 2001, Franco 2001).

5.2. The hectohertz Lorentzian

The hectohertz Lorentzian has been identified in several other neutron star LMXBs (SAX J1808.4-3658, 4U 1705–44; Wijnands & van der Klis 1998). Sunyaev & Revnivtsev (2000) use a sample of 9 BHCs and 9 neutron star LMXBs (including SAX J1808.4-3658, 4U 1705–44, 4U 0614+09 and 4U 1728–34) to show that neutron star systems show significant broad–band noise above several hundred Hz where BHC do not. The hectohertz Lorentzian is one of the contributers to this excess of power in SAX J1808.4-3658, 4U 1705–44, 4U 0614+09 and 4U 1728–34 and could be in the other sampled neutron star LMXBs.

The hectohertz Lorentzians could be related to the $\sim$ 67 Hz QPO in the BHC GRS 1915+105

(Morgan, Remillard & Greiner 1997) and the $\sim$ 300 Hz QPO in the BHC GRO J1655–40 (Remillard et al. 1999). These oscillations also have stable frequencies and fall in the same frequency range as the hectohertz Lorentzians we observe. However, these QPOs are much narrower ($Q \sim 5$ for the $\sim$ 300 Hz QPO and $Q \sim 20$ for the $\sim$ 67 Hz QPO) and have much weaker rms fractional amplitudes ($\sim$1 %). Models to explain these stable QPOs in the BHCs all invoke strong gravity near the central black hole (see for a review Cui, Chen & Zhang 2000).

Recently, Fragile, Mathews & Wilson (2001) made a tentative identification of the 9 Hz QPO in the BHC GRO J1655–40 (Remillard et al. 1999) with the orbital frequency at the Bardeen–Petterson transition radius (e.g. Bardeen & Petterson 1975). Based on the similarities between the hectohertz Lorentzian in the neutron star LMXBs and the 9 Hz QPO in GRO J1655–40 they also suggest this identification for the hectohertz Lorentzian. For 4U 0614+09 and 4U 1728–34 we can confirm that in indeed several properties of the hectohertz Lorentzian are quite similar to those of the 9 Hz QPO in GRO J1655–40. As in the case of the 9 Hz QPO, the hectohertz Lorentzian always has $Q < 3$ and for both features the characteristic frequency is nearly constant whilst the frequencies of other components change.

5.3. Comparison with BHCs and low–luminosity bursters

As noted in §1, if the two highest frequency QPOs in the BHCs could be identified with the lower and upper kilohertz QPO in the atoll sources (as suggested by respectively PBK99 and Nowak 2000), one would predict that in 4U 1728–34 and 4U 0614+09 the two high–frequency Lorentzians should be absent from the broad–band noise if the two kilohertz QPOs are present. Our results show a more complicated picture; when the two kilohertz QPOs are clearly present, then in addition to the zero–centered Lorentzian and the low–frequency Lorentzian, two more Lorentzian components are present, the BLN QPO and the hectohertz Lorentzian. These Lorentzians however have quite a special character. The BLN QPO is strongly connected with the zero–centered Lorentzian and seems to be part of the BLN (see §3.1), which is not clear for the two highest–frequency Lorentzians describing the broad–band noise in the BHCs. The hectohertz Lorentzian is almost constant in frequency with a frequency of about 150 Hz. The highest–frequency Lorentzian describing the broad–band noise in the BHCs might also be constant in frequency at about 30 Hz, but there is currently not enough data available for the BHCs to confirm this. The factor of $\sim$ 5 difference in frequency might then be caused by a scaling with the mass of the compact object which is about a factor of 5 lower for the neutron stars.

The power spectra of the low–luminosity bursters and BHCs studied in Nowak (2000) and BPK01 showed four Lorentzian components three of which in practice are zero–centered. The atoll sources 4U 1728–34 and 4U 0614+09 also show four Lorentzian components at low inferred mass accretion rates (intervals 1–8 of 4U 1728–34 and 1–4 of 4U 0614+09). So can we identify all four peaks in these intervals of 4U 1728–34 and 4U 0614+09 with the four peaks in the BHCs and the low–luminosity bursters? The first two Lorentzian components in the low–luminosity bursters, BHCs and the atoll sources 4U 1728–34 and 4U 0614+09 may have the same physical origin as they also show a similar relation between their respective characteristic frequencies (the WK99 relation, see Fig. 9, bottom panel). Interval 1 of 4U 0614+09 is almost identical to that of the low–luminosity bursters. However, because interval 1 of 4U 0614+09 is an extreme point in the current dataset available for 4U 0614+09, its two highest–frequency Lorentzians cannot be linked directly with the two highest frequency Lorentzians of intervals 2–4. More observations of 4U 0614+09 with a $\nu_{\rm band}$ between 0.3 and 1.4 Hz are needed to connect these points.

The third Lorentzian of the BHCs and low–luminosity bursters however, behaves completely differently from the third Lorentzian in 4U 1728–34 and 4U 0614+09 (except for interval 1). Where the characteristic frequency of the third Lorentzian in 4U 1728–34 and 4U 0614+09 (i.e. the hectohertz Lorentzian) is almost constant at about 150 Hz, the third Lorentzian in the BHCs and low–luminosity bursters varies over several orders of magnitude (Fig. 9, middle panel). Instead, the PBK99 relation as well as the relation between the characteristic frequency of the

third Lorentzian in the BHCs and low–luminosity bursters with $\nu_{\rm band}$ (Fig. 9, middle panel) suggest the identification of this Lorentzian with the lower kilohertz QPO that is present in intervals 10–17 of 4U 1728–34 and intervals 6–8 of 4U 0614+09.

Based on the similarity between the relation between the characteristic frequencies of the third and the fourth Lorentzians in the BHCs GX 339–4 and Cyg X–1 and the relation between the characteristic frequencies of the lower and upper kilohertz QPOs, Nowak (2000) suggested the identification of the fourth Lorentzian with the upper kilohertz QPO. Indeed the upper kilohertz QPO is also the fourth peak in the intervals at lower inferred mass accretion rates, where 4U 1728–34 and 4U 0614+09 mimic the BHCs most. However, the relation between the characteristic frequency of the fourth Lorentzian and $\nu_{\rm band}$ does not confirm this identification (see §4). For the low–luminosity bursters 1E 1724–3045 and GS 1826–24 studied in BPK01 the identification of the fourth peak with the upper kilohertz QPO is even harder (see §4). But keep in mind that due to the extensive data sets available for our two sources we are able to keep track of $\nu_{\rm band}$ through the transformation from zero–centered Lorentzian to BLN QPO. With less data, confusion might occur.

5.4. Summary

- The use of exactly the same fit function for 4U 0614+09 and 4U 1728–34 shows that these two atoll sources show a remarkably similar timing behaviour at luminosities that differ by a factor of 5.
- Interval 1 of 4U 0614+09 shows a remarkably similar power spectrum to that of the low–luminosity bursters. Unfortunately, this is an extreme point in the current dataset available for 4U 0614+09 and therefore the two highest frequency Lorentzians cannot be linked directly with the high frequency Lorentzians of the other intervals. More observations of 4U 0614+09 with a $\nu_{\rm band}$ between 0.3 and 1.4 Hz are needed to complete the picture.
- When the two kilohertz QPOs are clearly present, the low–frequency part of the power spectrum is too complicated to draw immediate conclusions from the nature of the components detected in any one power spectrum. The relation of characteristic frequency of respectively the two high–frequency Lorentzians with the characteristic frequency of the band–limited noise ($\nu_{\rm band}$) hints towards the identification of the second–highest frequency Lorentzian in the BHCs with the lower kilohertz QPO (as suggested by PBK99) but can not confirm the identification of the highest frequency Lorentzian with the upper kilohertz QPO (as suggested by Nowak 2000).
- When using $\nu_{\rm max}$ instead of the centroid frequency, the recently discovered hectohertz Lorentzians are almost stable in frequency.
- All Lorentzian components in 4U 0614+09 and 4U 1728–34 become broader as their frequency decreases. This might explain why many Lorentzians in other sources are zero–centered when present at low frequencies.
- The use of the multi–Lorentzian fit function clearly shows the presence of the band–limited noise QPO in 4U 0614+09 at frequencies where a broken power–law fit function has troubles. The similarity between the BLN QPO in 4U 0614+09 and 4U 1728–34 confirms the identification of the BLN QPO in 4U 0614+09.

6. Acknowledgements

This work was supported by NWO SPINOZA grant 08–0 to E.P.J. van den Heuvel, by the Netherlands Organization for Scientific Research (NWO), and by the Netherlands Research School for Astronomy (NOVA). This research has made use of data obtained through the High Energy Astrophysics Science Archive Research Center Online Service, provided by the NASA/Goddard Space Flight Center. We would like to thank Bob Shirey for providing us with a table of the Cir X–1 data.

REFERENCES

[Bardeen & Petterson 1975]Bardeen, J. M., & Petterson, J. A., 1975, ApJ, 195, L65

[Belloni et al. 1997]Belloni, T., van der Klis, M., Lewin, W.H.G. van Paradijs, J., Dotani, T.,

Mitsuda, K., Miyamoto, S., 1997, A&A, 322, 857

[1]Belloni, T., Psaltis, D., van der Klis, M., 2001, ApJ, submitted (BPK01)

[2]Cui, W., Chen, W., Zhang, S. N., in Proc. Meeting on the Lense–Thirring effect, ed. L. Z. Fang & R. Ruffini (singapore: World Scientific), in press (astro-ph/9811023)

[Di Salvo et al. 2001]Di Salvo, T., Méndez, M., van der Klis, M., Ford, E., Robba, N.R., 2001, ApJ, 546, 1107 (DS01)

[Ford et al. 2000]Ford, E. C., van der Klis, M., Méndez, M., Wijnands, R., Homan, J., Jonker, P. G., van Paradijs, J., 2000, ApJ, 537, 368

[3]Fragile, P. C., Mathews, G. J., Wilson, J. R., 2001, ApJ, 553, 955

[Franco 2001]Franco, L. M., 2001, ApJ, 554, 340

[Hasinger & van der Klis 1989]Hasinger, G., & van der Klis, M., 1989, A&A, 225, 79

[Homan et al. 2001]Homan, J., van der Klis, M., Jonker, P. G., Wijnands, R., Kuulkers, E., Méndez, M., Lewin, W. H. G., 2001, ApJ, submitted (astro-ph/0104323)

[Leahy et al. 1983]Leahy, D. A., Darbro, W., Elsner, R. F., Weisskopf, M. C., Kahn, S., Sutherland, P. G., Grindlay, J. E., 1983, ApJ, 266, 160

[4]Morgan, E.H., Remillard, R.A., Greiner, J., 1997, ApJ, 482, 993

[Nowak 2000]Nowak, M.A., 2000, MNRAS, 318, 361

[5]Psaltis, D., Belloni, T., van der Klis, M., 1999, ApJ, 520, 262 (PBK99)

[Remillard et al. 1999]Remillard, R.A., Morgan, E.H., McClintock, J.E., Bailyn, C.D., Orosz, J.A., 1999, ApJ, 522, 397

[Schultz 1999]Schultz, N. S., 1999, ApJ, 511, 304

[Shirey 1998]Shirey, R. E., 1998, Ph. D. thesis, MIT (astro-ph/9806346)

[Sunyaev & Revnivtsev 2000]Sunyaev, R., & Revnivtsev, M., 2000, A&A, 358, 617

[van der Klis 1994a]van der Klis, M., 1994a, A&A, 283, 469

[van der Klis 1994b]van der Klis, M., 1994b, ApJ-Suppl., 92, 511

[van der Klis 1995]van der Klis, M., 1995, in "X-ray binaries", eds. Lewin, W.H.G., Van Paradijs, J., & Van den Heuvel, E.P.J., Cambridge Univ. Press., Cambridge, p252.

[van der Klis 2000]van der Klis, M. 2000, ARA&A, 38, 717

[van Straaten et al. 2000]van Straaten, S., Ford, E.C., van der Klis, M., Méndez, M., Kaaret, P. 2000, ApJ, 540, 1049 (vS00)

[van Straaten et al. 2001]van Straaten, S., van der Klis, M., Kuulkers, E., Méndez, M., 2001, ApJ, 551, 907

[Wijnands & van der Klis 1998]Wijnands, R., van der Klis, M., 1998, ApJ, 507, L63

[Wijnands & van der Klis 1999]Wijnands, R., van der Klis, M., 1999, ApJ, 514, 939 (WK99)

[Zhang et al. 1993]Zhang, W., Giles, A.B., Jahoda, K., Soong, Y., Swank, J.H., Morgan, E.H., 1993, SPIE, 2006, 324

AAS LaTeX macros v5.0.

TABLE 1

CHARACTERISTIC FREQUENCIES OF THE MULTI–LORENTZIAN FIT FOR 4U 1728–34 & 4U 0614+09

Interval Number	zc Lorentzian $\nu_{\rm BLNZERO}$ (Hz)	BLN QPO $\nu_{\rm BLNQPO}$ (Hz)	LF Lorentzian $\nu_{\rm LF}$ (Hz)	hHz Lorentzian $\nu_{\rm hHz}$ (Hz)	Lower kHz QPO $\nu_{\rm lowerkHz}$ (Hz)	Upper kHz QPO $\nu_{\rm upperkHz}$ (Hz)
			4U 1728–34			
1	1.976±0.057	–	11.47±0.16	178±35	–	399±13
2	2.077±0.046	–	11.75±0.13	173±22	–	416±12
3	2.983±0.083	–	16.19±0.25	203±28	–	497±14
4	3.976±0.060	–	19.72±0.17	175.0±5.3	–	519.1±5.1
5	4.184±0.059	–	20.12±0.16	175.3±6.1	–	521.4±5.2
6	4.56±0.12	–	21.56±0.33	198±13	–	531.7±8.0
7	12.3±0.9	–	27.5±1.0	175±14	–	705.7±8.1
8	16.63±0.60	–	31.29±0.63	152.3±6.5	–	732.6±3.1
9	14.2±4.5	16.20±0.46	36.26±0.47	130.7±5.9	–	791.1±2.2
10	19.5±2.3	19.39±0.31	42.14±0.77	136.9±4.5	513±18	849.5±2.0
11	21.2±2.2	20.96±0.23	45.52±0.66	127.3±3.2	561±11	875.7±1.6
12	18.8±2.6	23.08±0.29	46.70±0.91	129.7±3.6	604±14	907.6±2.5
13	11.6±1.2	30.61±0.53	–	130.9±2.9	680±10	951.0±3.7
14	16.9±1.8	40.64±0.47	–	147.1±5.3	754.0±3.7	1056.2±8.2
15	13.3±1.0	42.21±0.29	–	164.3±5.3	775.3±1.7	1107.5±7.2
16	14.5±1.5	43.39±0.32	–	151.6±7.8	819.9±4.1	1134±12
17	$12.9^{+5.7}_{-3.5}$	43.21±0.98	–	224±27	879.2±3.0	1161±16
18	–	33.4±3.6[1]	–	–	–	–
19	–	20.9±3.5[1]	–	–	–	–
			4U 0614+09			
1	0.3054±0.0046	–	2.057±0.014	–	19.97±0.46[1]	233.4±8.6[1]
2	1.434±0.020	–	9.558±0.076	157±12	–	369.7±7.5
3	3.47±0.14	–	16.39±0.43	153±12	–	481±15
4	10.74±0.71	–	25.38±0.76	153.6±7.7	–	629.6±4.3
5	$7.0^{+2.6}_{-1.7}$	17.54±0.46	37.70±0.63	121.8±5.3	–	755.8±4.1
6	9.1±1.7	21.11±0.37	$44.4^{+1.2}_{-0.6}$	121.0±3.3	517±12	833.2±4.2
7	$11.4^{+3.0}_{-2.0}$	26.17±0.42	–	132.3±4.7	607.9±1.7	925.9±3.5
8	21.0±5.0	31.17±0.41	–	148.9±5.0	754.8±2.4	1137.1±7.0
9	–	23.77±0.92[1]	–	117.5±1.5	–	1273.6±9.5

NOTE.—Listed are the characteristic frequencies ($\equiv \nu_{\rm max}$) of the different Lorentzians described in §3. The quoted errors in $\nu_{\rm max}$ use $\Delta\chi^2 = 1.0$.

[1] The identification of this Lorentzian is not clear, see §3.

TABLE 2

Q VALUES OF THE MULTI–LORENTZIAN FIT FOR 4U 1728–34 & 4U 0614+09

Interval Number	BLN QPO	LF Lorentzian	hHz Lorentzian	Lower kHz QPO	Upper kHz QPO
			4U 1728–34		
1	–	0.589±0.037	0.03±0.15	–	$1.66^{+0.64}_{-0.41}$
2	–	0.578±0.030	0.09±0.11	–	1.46±0.26
3	–	0.437±0.029	0.51±0.14	–	1.77±0.42
4	–	0.594±0.021	0.769±0.073	–	1.81±0.13
5	–	0.623±0.020	0.652±0.061	–	1.76±0.13
6	–	0.634±0.039	0.58±0.10	–	2.29±0.30
7	–	2.04±0.80	0.52±0.17	–	4.29±0.59
8	–	2.17±0.44	0.445±0.083	–	4.23±0.21
9	$0.90^{+0.32}_{-0.14}$	2.64±0.38	0.256±0.062	–	5.30±0.22
10	1.60±0.21	2.52±0.44	0.545±0.074	$5.4^{+3.6}_{-2.0}$	6.29±0.29
11	$1.64^{+0.25}_{-0.17}$	$3.8^{+1.1}_{-0.7}$	0.603±0.058	$6.5^{+4.0}_{-1.8}$	6.62±0.22
12	1.62±0.25	3.44±0.88	0.762±0.086	4.29±0.98	6.78±0.38
13	0.690±0.059	–	1.12±0.12	3.89±0.68	6.04±0.45
14	1.78±0.18	–	1.44±0.22	6.21±0.47	6.9±1.1
15	1.99±0.11	–	1.53±0.24	7.52±0.37	7.9±1.0
16	2.20±0.16	–	1.37±0.23	4.96±0.20	10.5±2.0
17	1.67±0.28	–	1.11±0.46	13.2±1.3	$10.7^{+5.5}_{-3.7}$
18	0.62±0.18[1]	–	–	–	–
19	0.68±0.22[1]	–	–	–	–
			4U 0614+09		
1	–	0.504±0.017	–	0.057±0.039[1]	0.512±0.070[1]
2	–	0.464±0.0177	0.252±0.058	–	1.52±0.21
3	–	0.555±0.065	0.61±0.14	–	1.94±0.38
4	–	0.98±0.22	0.36±0.10	–	3.66±0.30
5	0.81±0.17	$6.2^{+4.3}_{-2.4}$	0.217±0.067	–	4.34±0.29
6	1.04±0.14	6^{+14}_{-3}	0.576±0.079	$5.9^{+3.1}_{-1.6}$	5.17±0.34
7	1.44±0.19	–	0.79±0.11	13^{+10}_{-3}	11.1±1.2
8	1.59±0.15	–	1.27±0.18	10.5±1.2	7.02±0.86
9	0.635±0.059[1]	–	2.79±0.27	–	10.9±2.9

NOTE.—Listed are the Q values ($\equiv \nu_0/2\Delta$) of the different Lorentzians described in §3. The quoted errors in Q use $\Delta\chi^2 = 1.0$.

[1] The identification of this Lorentzian is not clear, see §3.

TABLE 3

INTEGRATED FRACTIONAL RMS OF THE MULTI–LORENTZIAN FIT FOR 4U 1728–34 & 4U 0614+09

Interval Number	zc Lorentzian rms (%)	BLN QPO rms (%)	LF Lorentzian rms (%)	hHz Lorentzian rms (%)	Lower kHz QPO rms (%)	Upper kHz QPO rms (%)
			4U 1728–34			
1	13.32±0.17	–	14.43±0.30	13.7±1.2	–	9.1±1.4
2	13.11±0.14	–	14.46±0.25	13.17±0.80	–	9.64±0.89
3	13.08±0.19	–	14.56±0.26	11.8±1.3	–	10.72±1.28
4	13.82±0.10	–	13.47±0.15	10.67±0.34	–	12.10±0.32
5	13.878±0.093	–	13.17±0.14	11.13±0.35	–	11.82±0.34
6	13.89±0.17	–	13.00±0.27	11.71±0.64	–	10.90±0.61
7	15.47±0.49	–	$5.8^{+1.4}_{-0.9}$	12.47±0.74	–	12.07±0.56
8	14.93±0.24	–	4.80±0.51	10.74±0.36	–	12.38±0.21
9	11.2±2.6	$6.2^{+4.0}_{-1.7}$	4.83±0.39	$12.23^{+0.39}_{-0.78}$	–	11.95±0.17
10	11.68±0.82	5.03±0.75	3.99±0.42	10.05±0.36	3.02±0.52	10.81±0.19
11	11.22±0.69	5.18±0.59	2.87±0.38	9.19±0.36	2.91±0.34	10.43±0.13
12	9.90±0.77	5.89±0.67	3.09±0.40	8.93±0.37	4.50±0.37	9.96±0.22
13	6.12±0.38	8.46±0.33	–	6.83±0.23	5.45±0.38	8.20±0.24
14	5.73±0.26	5.41±0.25	–	4.68±0.24	6.92±0.21	5.33±0.32
15	4.36±0.13	5.16±0.12	–	3.91±0.19	7.01±0.12	4.50±0.21
16	3.92±0.16	4.73±0.13	–	3.60±0.20	7.61±0.13	3.15±0.26
17	2.91±0.41	4.49±0.29	–	3.82±0.46	5.71±0.22	3.41±0.50
18	–	2.77±0.18[1]	–	–	–	–
19	–	2.21±0.20[1]	–	–	–	–
			4U 0614+09			
1	17.55±0.11	–	19.73±0.23	–	20.96±0.37[1]	16.18±0.50[1]
2	16.29±0.11	–	18.90±0.18	17.42±0.82	–	12.7±1.0
3	17.45±0.38	–	17.28±0.64	17.6±1.2	–	16.1±1.2
4	17.45±0.63	–	10.8±1.3	18.84±0.80	–	16.90±0.53
5	$7.8^{+1.8}_{-1.1}$	11.2±1.2	$3.57^{+0.89}_{-0.53}$	19.97±0.53	–	16.34±0.37
6	$8.5^{+1.0}_{-0.7}$	10.64±0.72	$3.3^{+1.2}_{-0.5}$	16.34±0.48	5.55±0.67	14.42±0.34
7	$7.8^{+1.0}_{-0.6}$	9.54±0.62	–	12.98±0.46	$9.45^{+0.92}_{-0.31}$	10.66±0.42
8	5.50±0.77	8.32±0.39	–	9.07±0.40	9.21±0.35	10.31±0.43
9	–	6.09±0.16[1]	–	6.33±0.21	–	5.27±0.46

NOTE.—Listed are the values of the integrated fractional rms (over the full PCA energy band) of the different Lorentzians described in §3. The quoted errors in the rms use $\Delta\chi^2 = 1.0$.

[1] The identification of this Lorentzian is not clear, see §3.

TABLE 4

χ^2/DOF OF THE MULTI–LORENTZIAN VERSUS THE BROKEN POWER–LAW FIT FOR 4U 1728–34 & 4U 0614+09

Interval Number	Multi–Lorentzian fit χ^2 (dof)	Broken power–law fit χ^2 (dof)
	4U 1728–34	
1	295 (133)	241 (131)
2	382 (133)	273 (131)
3	198 (133)	270 (131)
4	546 (133)	587 (131)
5	485 (133)	538 (131)
6	257 (133)	267 (131)
7	175 (136)[1]	219 (134)[1]
8	208 (136)[1]	282 (131)
9	196 (133)[1]	254 (131)
10	234 (130)[1]	275 (131)[1]
11	206 (130)[1]	241 (131)[1]
12	159 (130)[1]	192 (131)[1]
13	198 (136)[2]	181 (134)[2]
14	190 (134)[2]	203 (132)[2]
15	308 (134)[2]	305 (132)[2]
16	348 (134)[2]	348 (132)[2]
17	184 (134)[2]	191 (132)[2]
18	181 (139)	179 (139)
19	188 (139)	184 (139)
	4U 0614+09	
1	245 (142)	217 (140)
2	258 (142)	308 (140)
3	194 (142)	207 (140)
4	175 (142)	177 (140)
5	164 (142)[1]	168 (143)[1]
6	154 (139)[1]	168 (137)[1]
7	179 (142)[1]	191 (140)[1]
8	118 (143)[2]	129 (144)[2]
9	191 (145)[1]	183 (144)[1]

NOTE.—Listed are the χ^2/dof of the multi–Lorentzian fit and the broken power–law fit for 4U 1728–34 & 4U 0614+09. The values of χ^2/dof for the broken power–law fit of 4U 1728–34 are from DS01.

[1] For this interval the χ^2/dof is calculated fixing the parameters of the upper kilohertz QPO (see §3).

[2] For this interval the χ^2/dof is calculated fixing the parameters of both kilohertz QPOs (see §3).

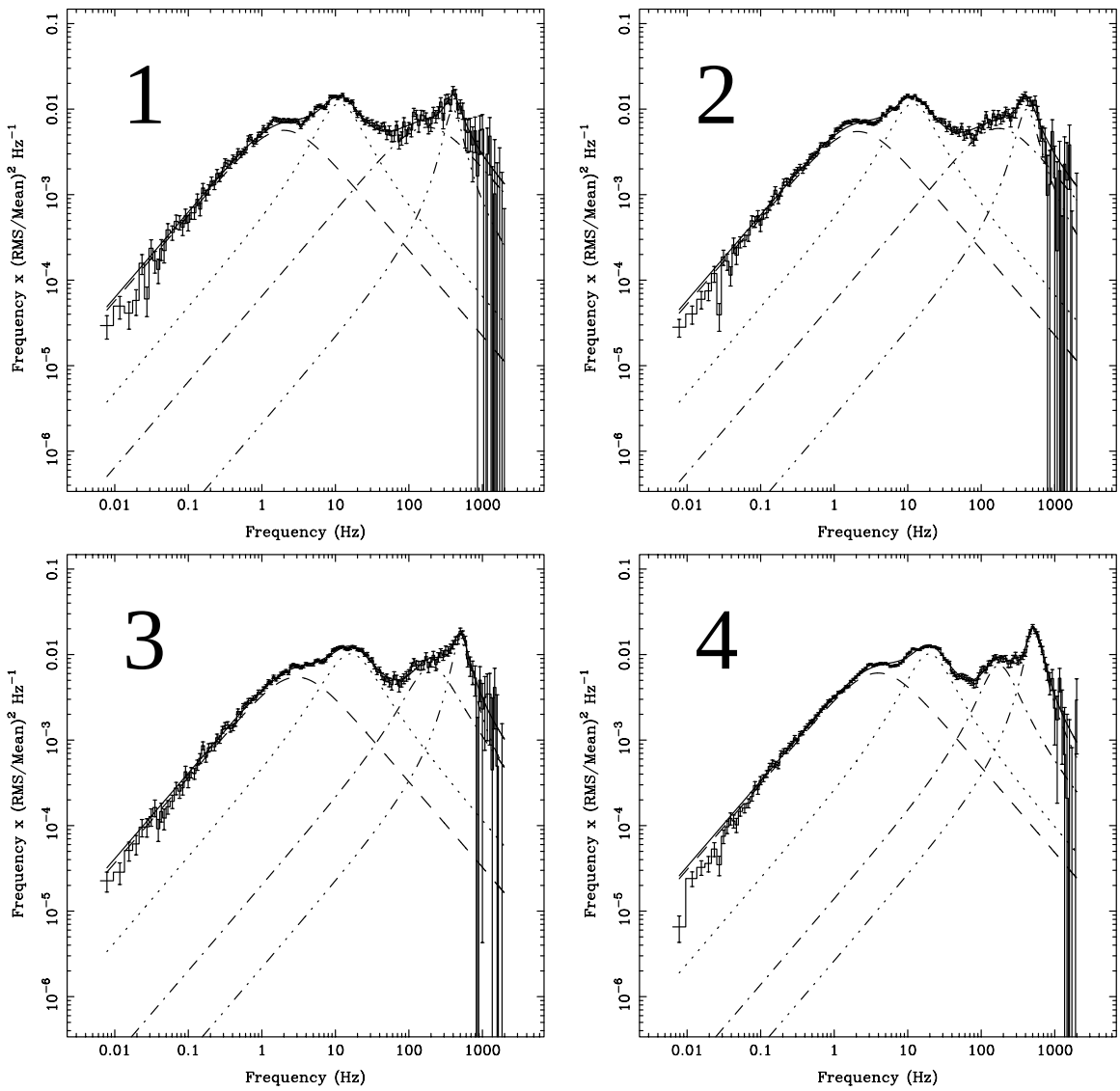

Fig. 1.— Power spectra and fit functions in the power spectral density times frequency representation (see §2) for 4U 1728–34. The different lines mark the individual Lorentzian components of the fit. The dashed lines mark both the BLN and the BLN QPO (§3.1), the dotted lines the low–frequency Lorentzian (§3.2), the dash–dotted line the hectohertz Lorentzian (§3.3) and the dash–dot–dot–dotted line both kilohertz QPOs (§3.4). In intervals 14–19 also a power–law is included to fit the VLFN. Interval numbers are indicated.

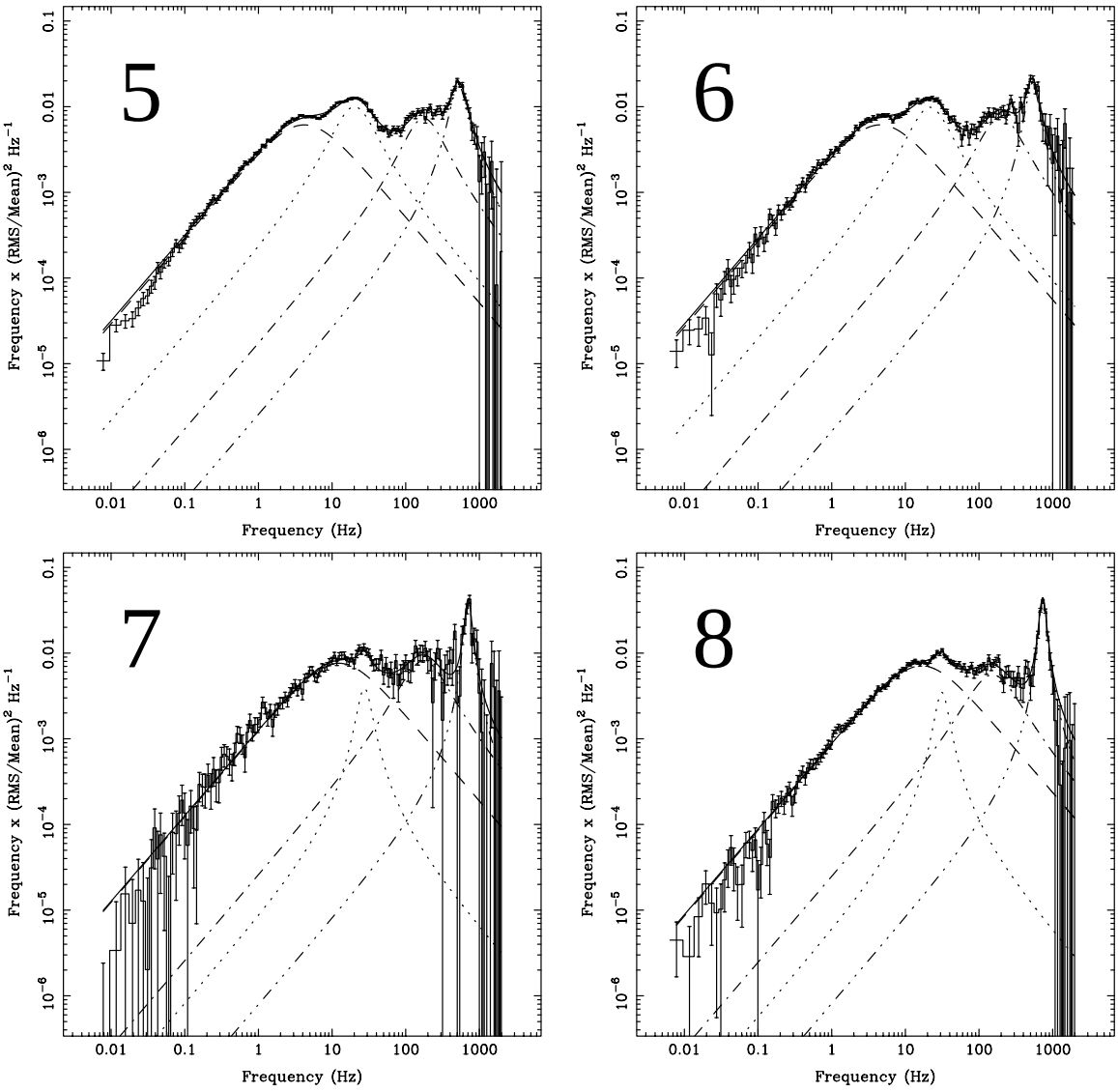

Fig. 1.— Continued

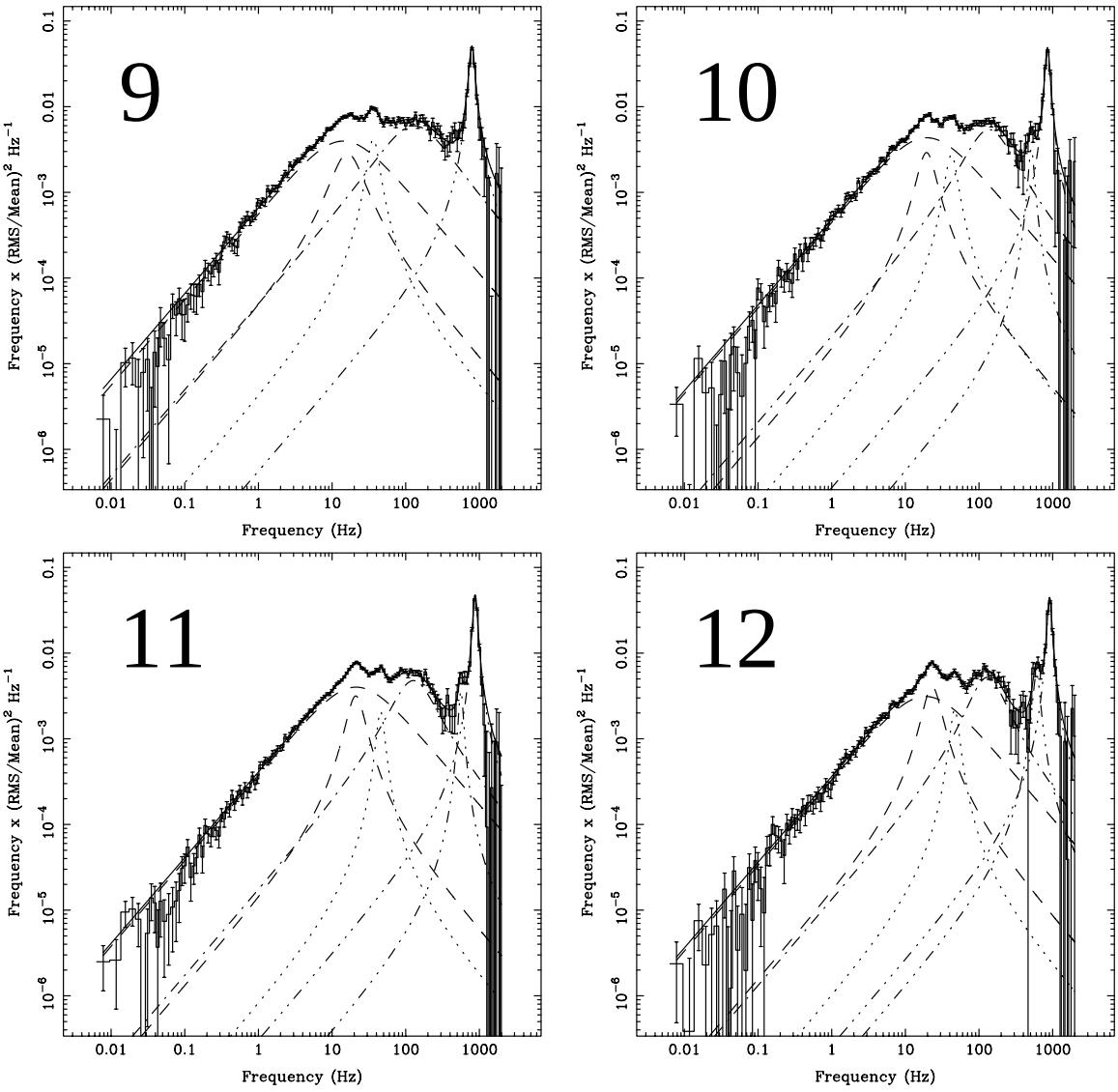

Fig. 1.— Continued

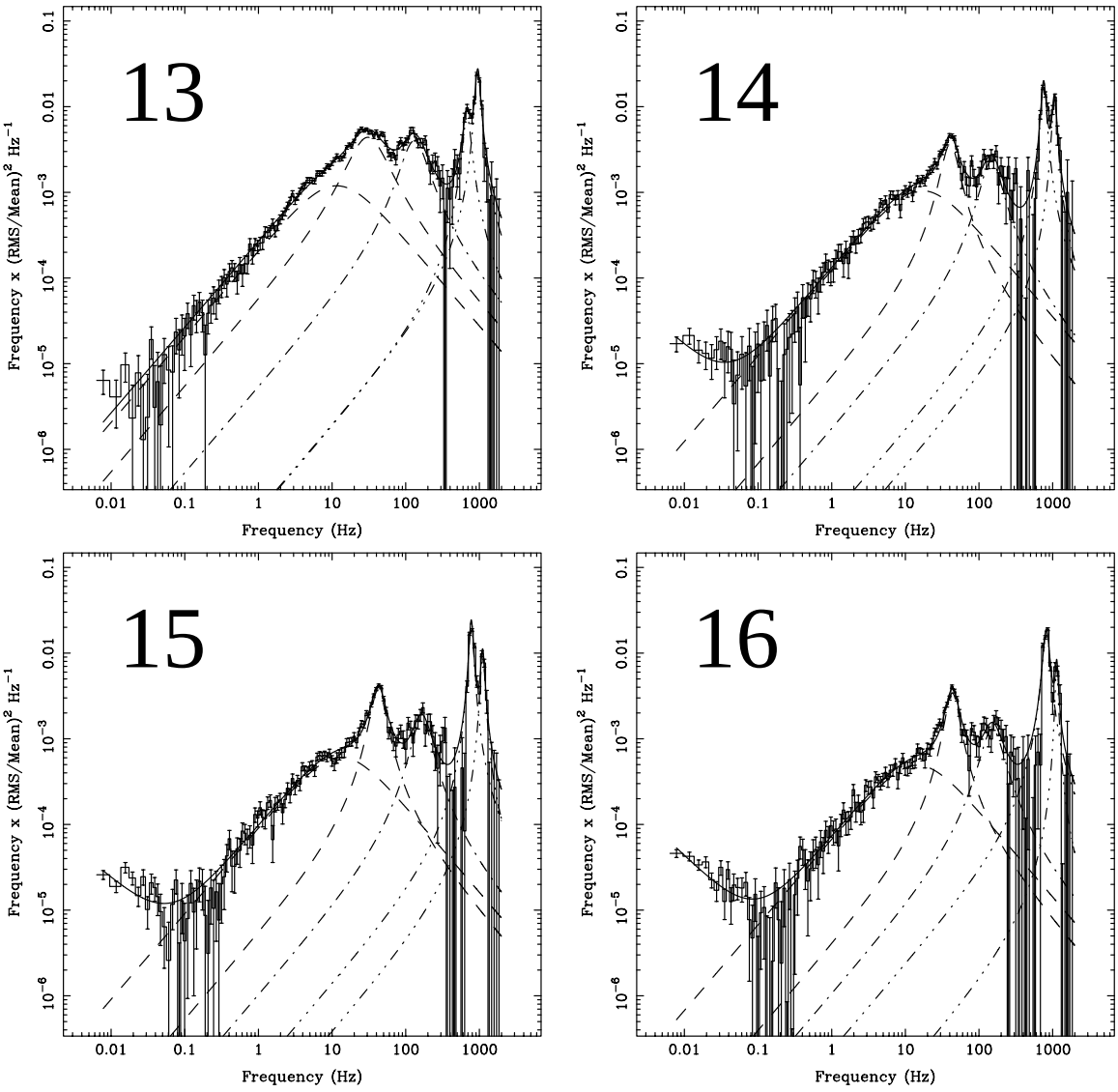

Fig. 1.— Continued

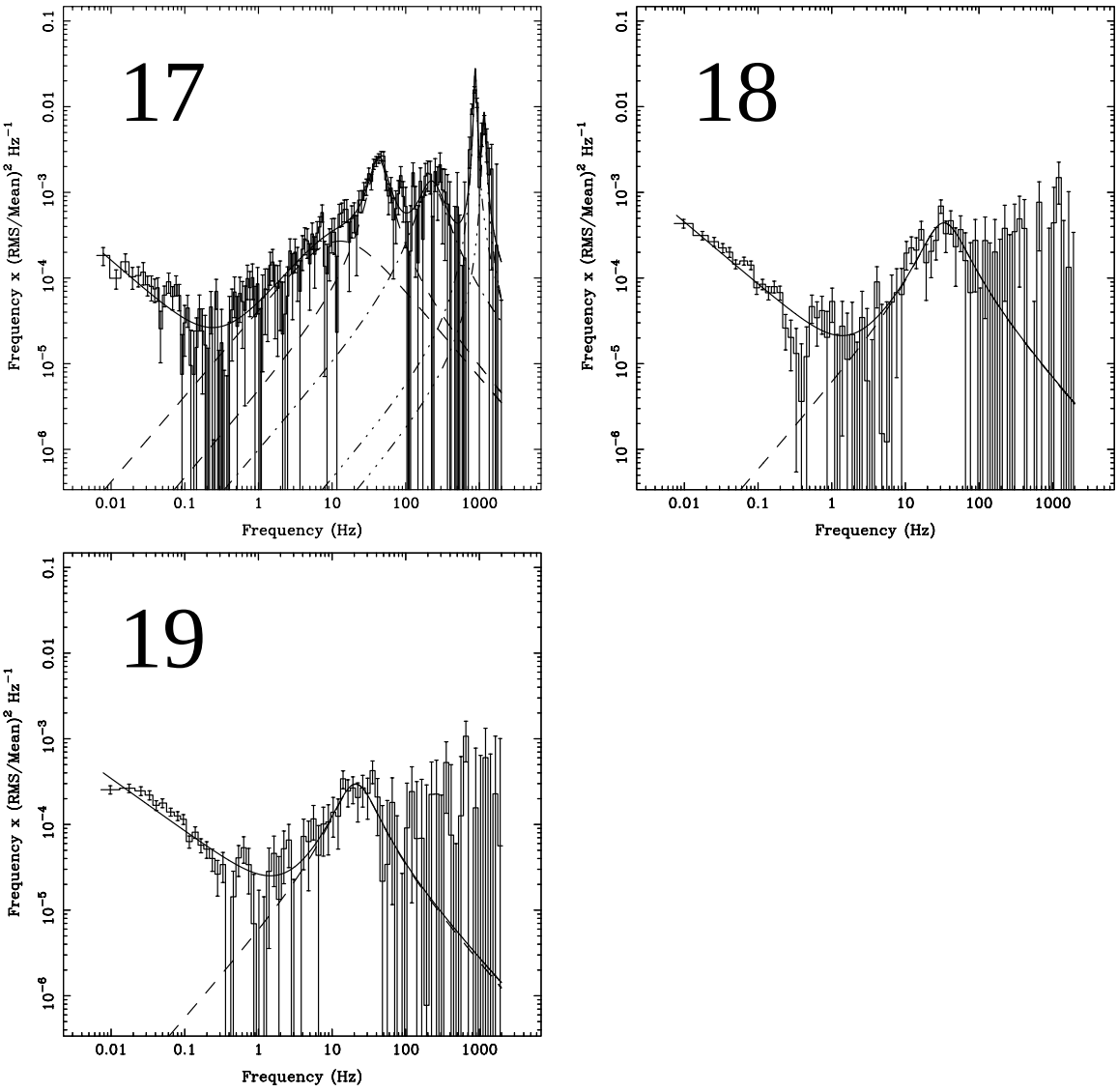

Fig. 1.— Continued

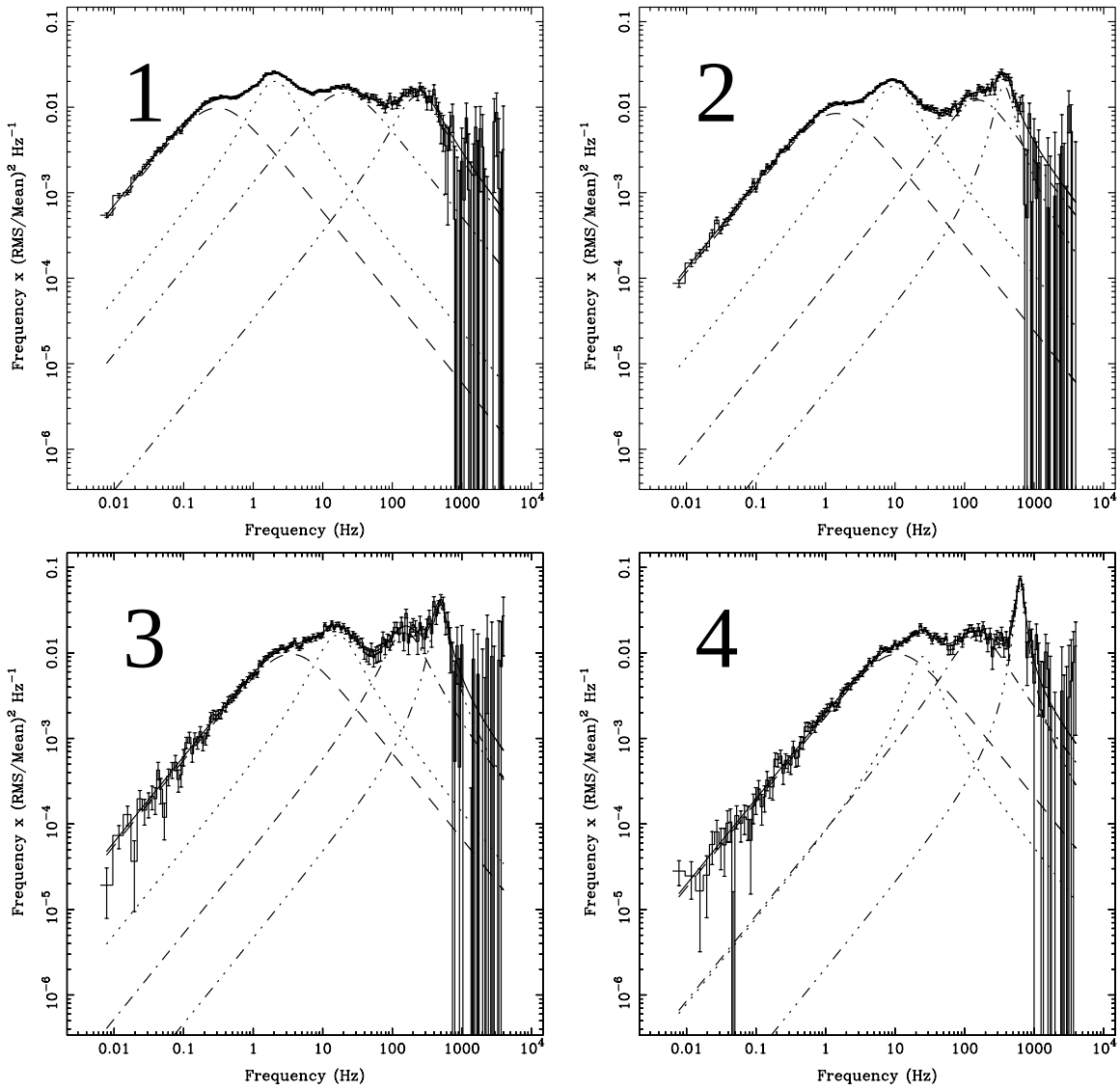

Fig. 2.— Power spectra and fit functions in the power spectral density times frequency representation (see §2) for 4U 0614+09. The different lines mark the individual Lorentzian components of the fit. The dashed lines mark both the BLN and the BLN QPO (§3.1), the dotted lines the low–frequency Lorentzian (§3.2), the dash–dotted line the hectohertz Lorentzian (§3.3) and the dash–dot–dot–dotted line both kilohertz QPOs (§3.4). In intervals 7 and 8 also a power–law is included to fit the VLFN. In interval 1 the identification of the two highest frequency Lorentzians is unclear (see §3.4). Interval numbers are indicated.

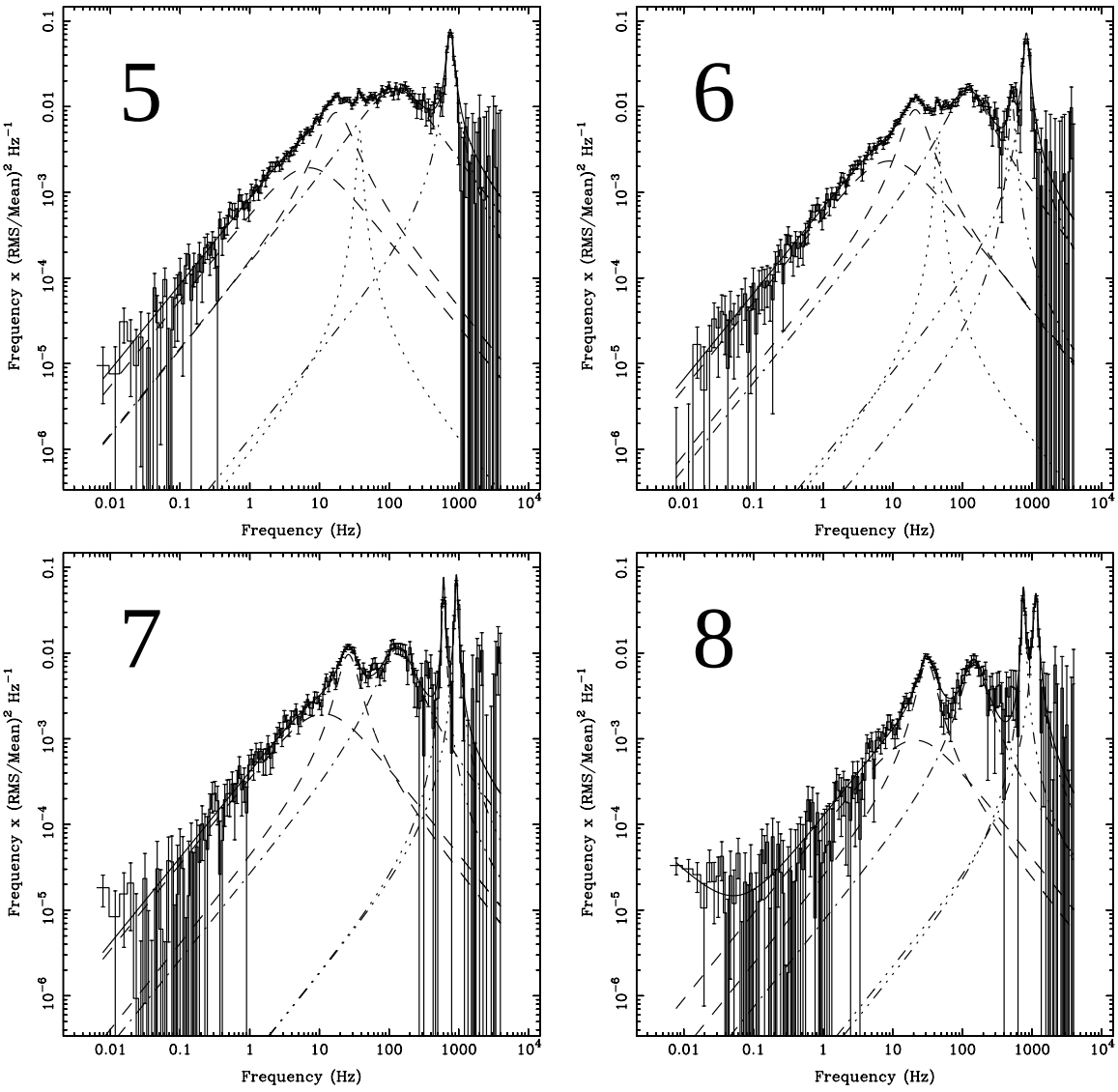

Fig. 2.— Continued

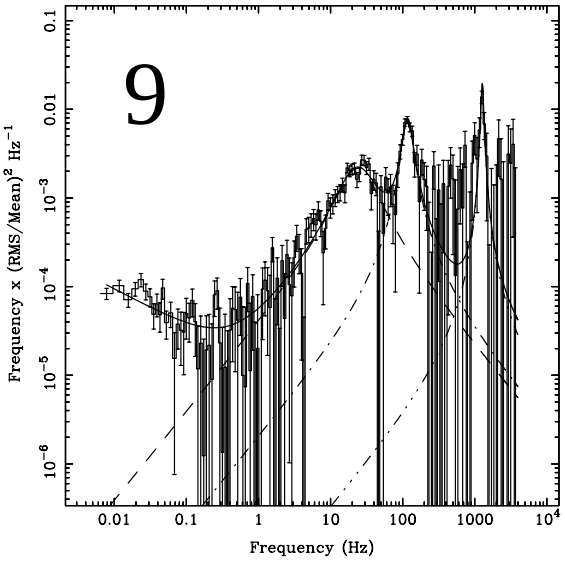

Fig. 2.— Continued

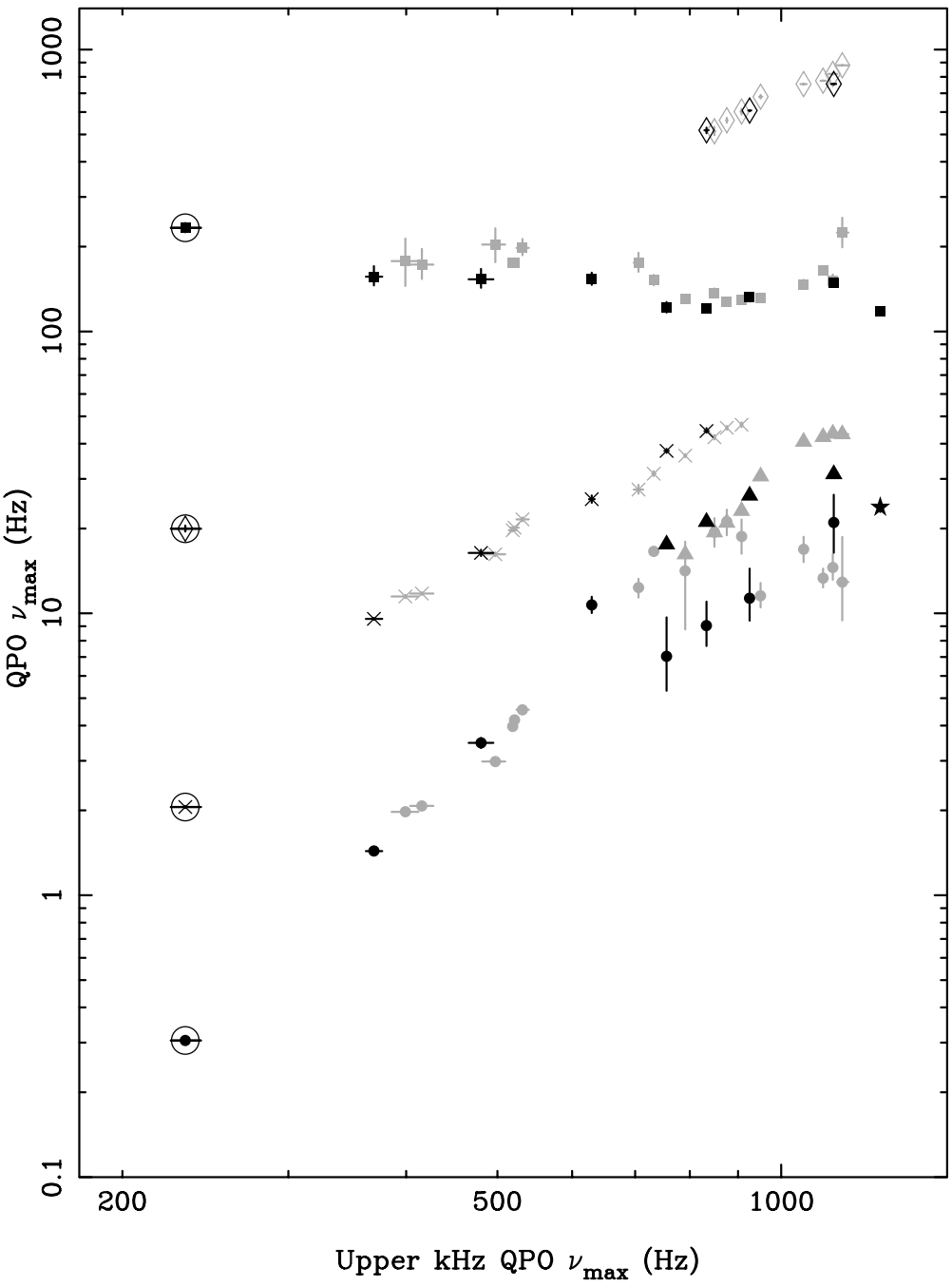

Fig. 3.— Correlations between the characteristic frequencies ($\equiv \nu_{\rm max}$) of the several Lorentzians used to fit the power spectra of 4U 1728–34 and 4U 0614+09 and the $\nu_{\rm max}$ of the Lorentzian identified as the upper kilohertz QPO. The grey symbols are the 4U 1728–34 points, the black symbols the 4U 0614+09 points. The circles mark the BLN (zero–centered Lorentzian), the triangles the BLN QPO, the x–ses the low–frequency Lorentzian, the squares the hectohertz Lorentzian and the diamonds the lower kilohertz QPO. The circled points are from interval 1 of 4U 0614+09, for which the fourth Lorentzian can be identified as either the upper kilohertz QPO or the hectohertz Lorentzian (see §3). We use the parameters of this Lorentzian both for the upper kilohertz QPO and for the hectohertz Lorentzian. The star marks the one Lorentzian in interval 9 of 4U 0614+09 for which the identification is not clear (see §3.1). The other Lorentzians for which the identification is not clear (intervals 18 and 19 of 4U 1728–34) are not in this plot as the upper kilohertz QPO is absent in those intervals.

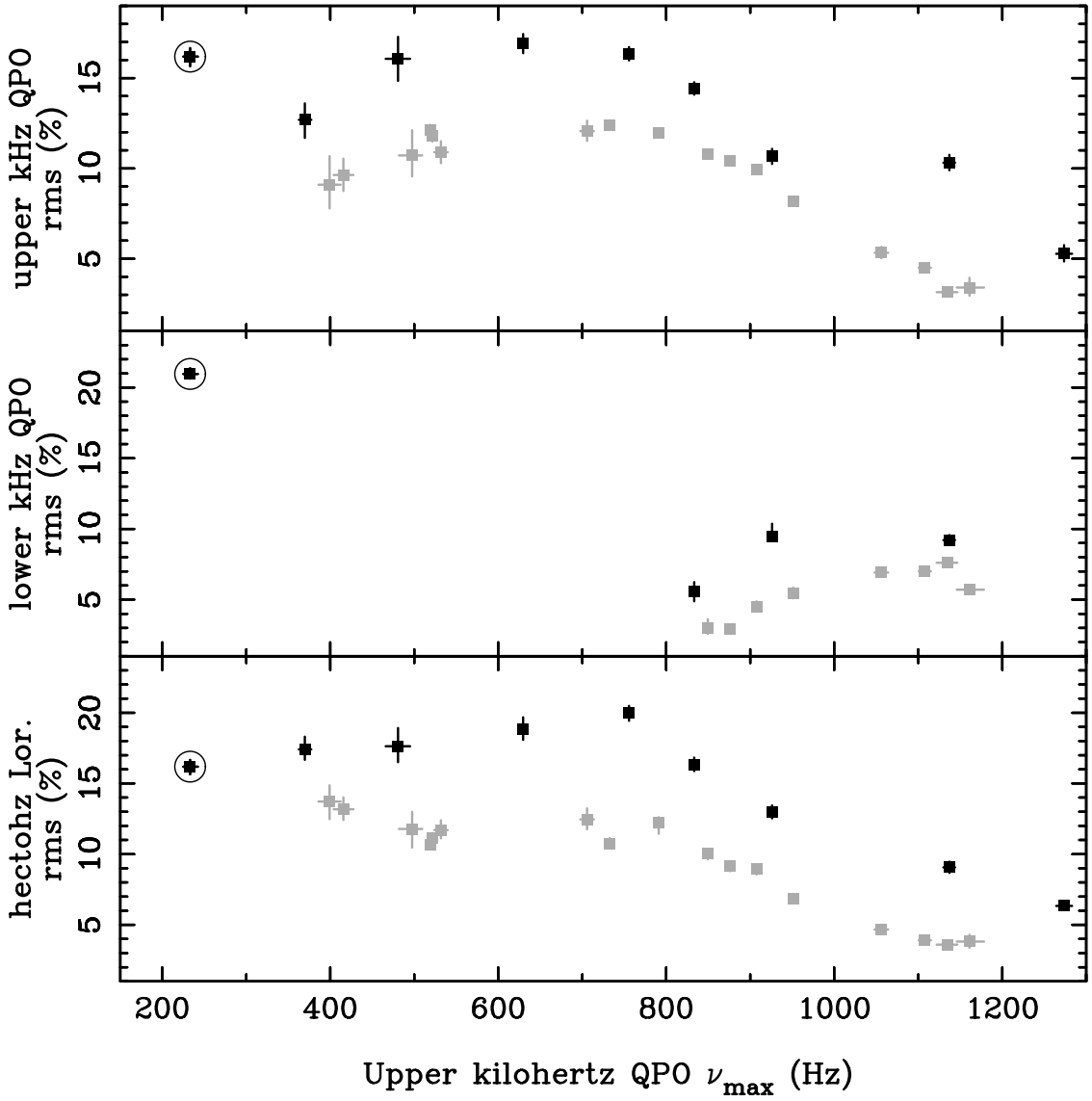

Fig. 4.— The fractional rms (over the full PCA energy band) of the hectohertz Lorentzian, the lower and upper kilohertz QPOs versus the $\nu_{\rm max}$ of the upper kilohertz QPO. The grey symbols are the 4U 1728–34 points, the black symbols the 4U 0614+09 points. The circled points are from interval 1 of 4U 0614+09, for which the fourth Lorentzian can be identified as either the upper kilohertz QPO or the hectohertz Lorentzian (see §3). We use the parameters of this Lorentzian both for the upper kilohertz QPO and for the hectohertz Lorentzian.

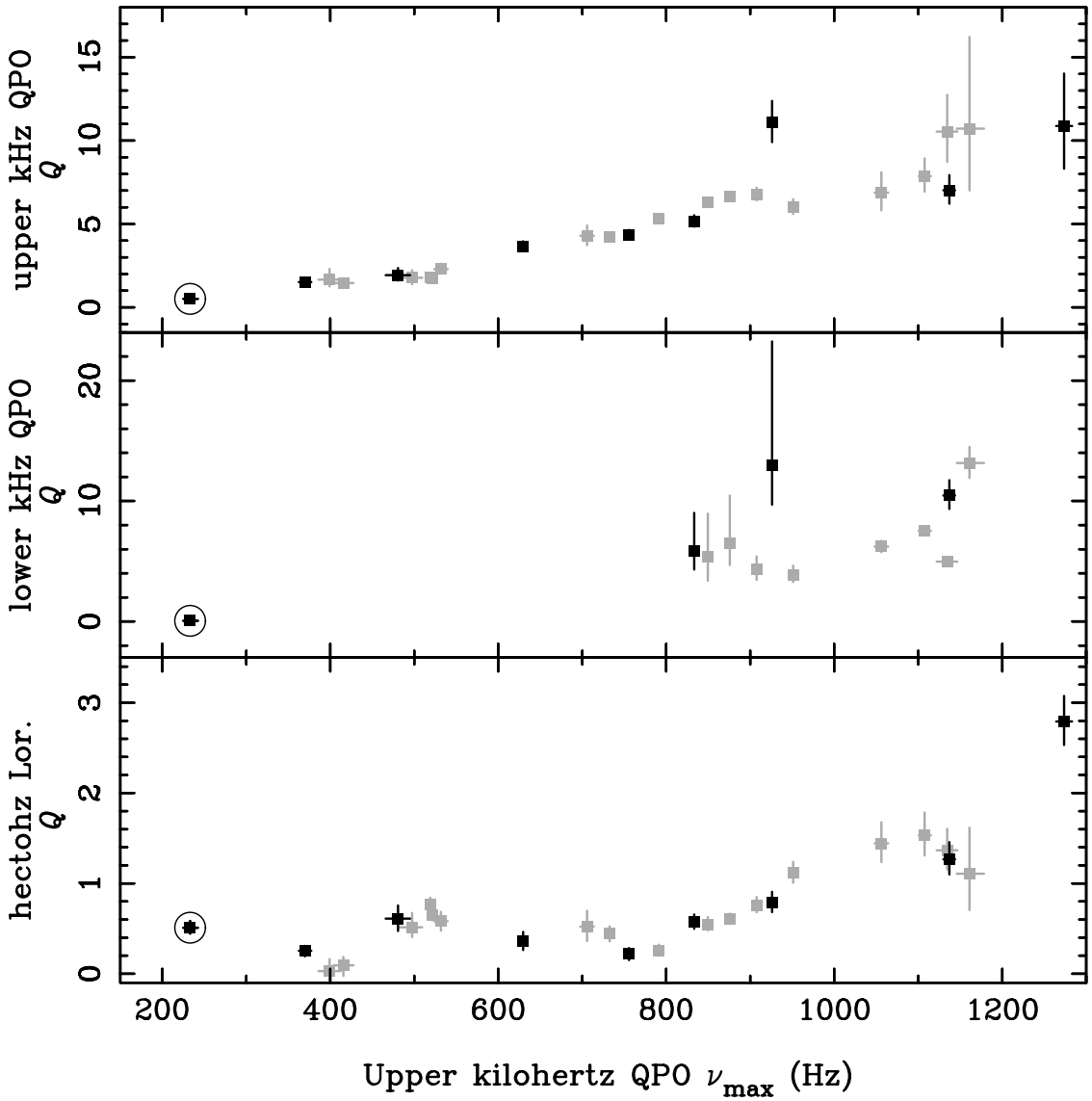

Fig. 5.— The Q values ($\equiv \nu_0/2\Delta$) of the hectohertz Lorentzian, the lower and upper kilohertz QPOs versus the $\nu_{\rm max}$ of the upper kilohertz QPO. The grey symbols are the 4U 1728–34 points, the black symbols the 4U 0614+09 points. The circled points are from interval 1 of 4U 0614+09, for which the fourth Lorentzian can be identified as either the upper kilohertz QPO or the hectohertz Lorentzian (see §3). We use the parameters of this Lorentzian both for the upper kilohertz QPO and for the hectohertz Lorentzian.

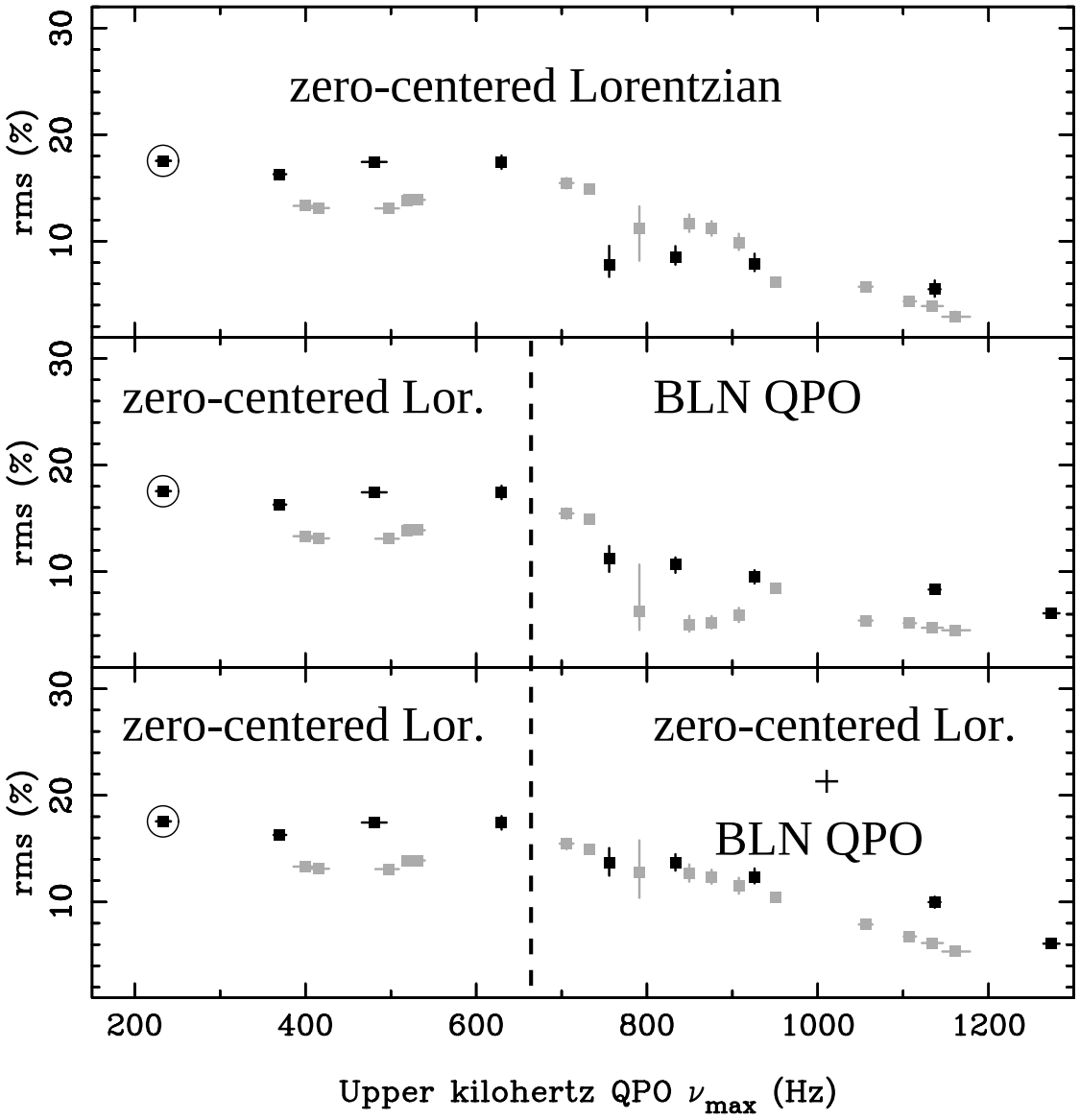

Fig. 6.— The fractional rms of the BLN versus $\nu_{\rm upperkHz}$. In the top panel we plot the rms of the zero–centered Lorentzian vs. $\nu_{\rm upperkHz}$. In the top panel we plot the fractional rms of the zero–centered Lorentzian. In the middle panel we plot the fractional rms of the BLN QPO when it is present, and the fractional rms of the zero–centered Lorentzian when it is not. In the bottom panel finally we plot the fractional rms of the zero–centered Lorentzian and the BLN QPO together. The grey symbols mark the 4U 1728–34 points, the black symbols the 4U 0614+09 points. The circled points are from interval 1 of 4U 0614+09, for which the fourth Lorentzian can be identified as either the upper kilohertz QPO or the hectohertz Lorentzian (see §3). We use the parameters of this Lorentzian both for the upper kilohertz QPO and for the hectohertz Lorentzian.

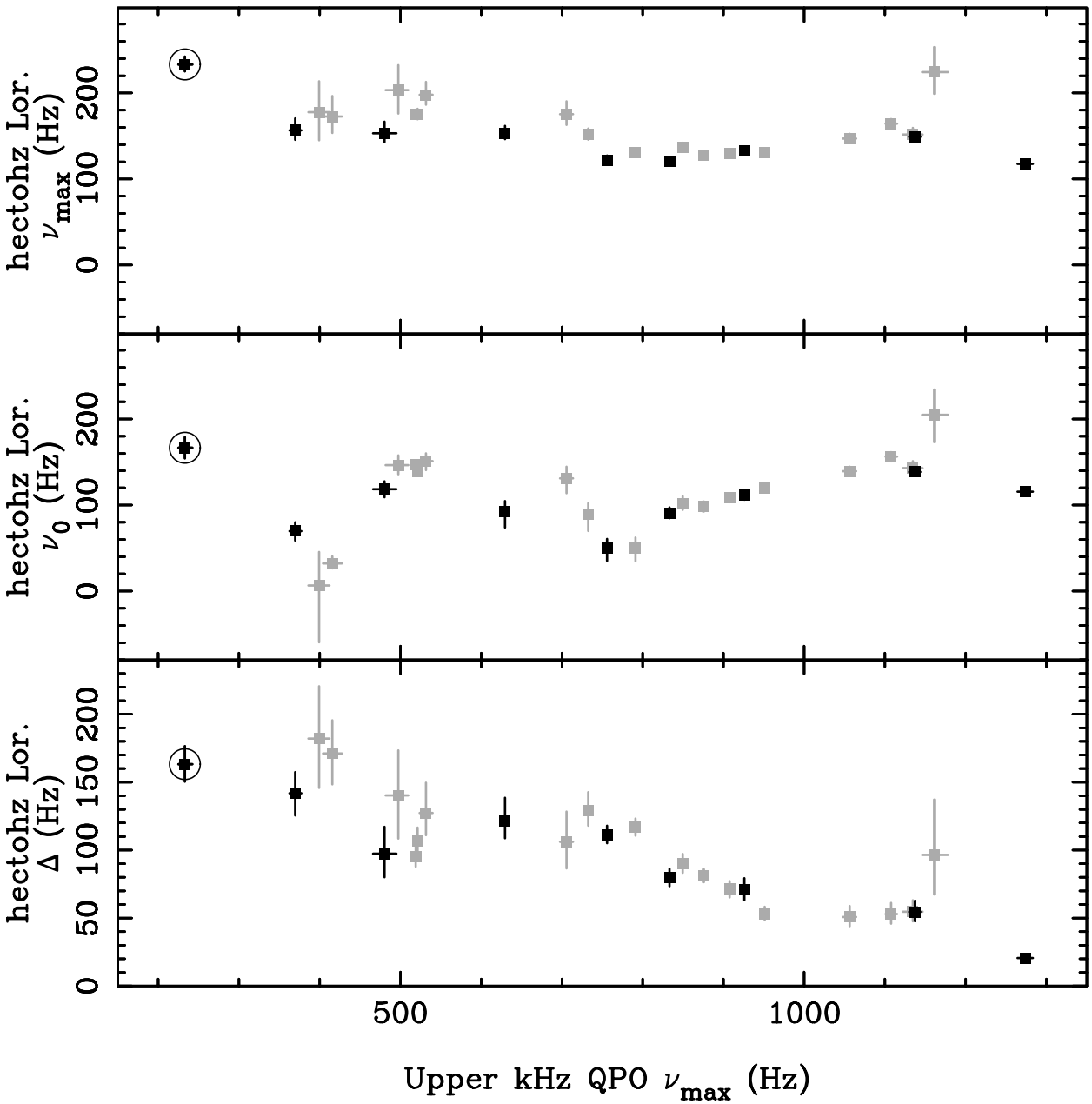

Fig. 7.— $\nu_{\rm max}$, ν_0 and Δ of the hectohertz Lorentzian versus the $\nu_{\rm max}$ of the upper kilohertz QPO. The grey symbols mark the 4U 1728–34 points, the black symbols the 4U 0614+09 points. The characteristic frequency of the hectohertz Lorentzian is either dominated by ν_0, Δ or both and therefore the use of $\nu_{\rm max}$ as the characteristic frequency of the hectohertz Lorentzian most clearly shows the near constant frequency of this feature. For comparison the top two panels are plotted on the same scale. The circled points are from interval 1 of 4U 0614+09, for which the fourth Lorentzian can be identified as either the upper kilohertz QPO or the hectohertz Lorentzian (see §3). We use the parameters of this Lorentzian both for the upper kilohertz QPO and for the hectohertz Lorentzian.

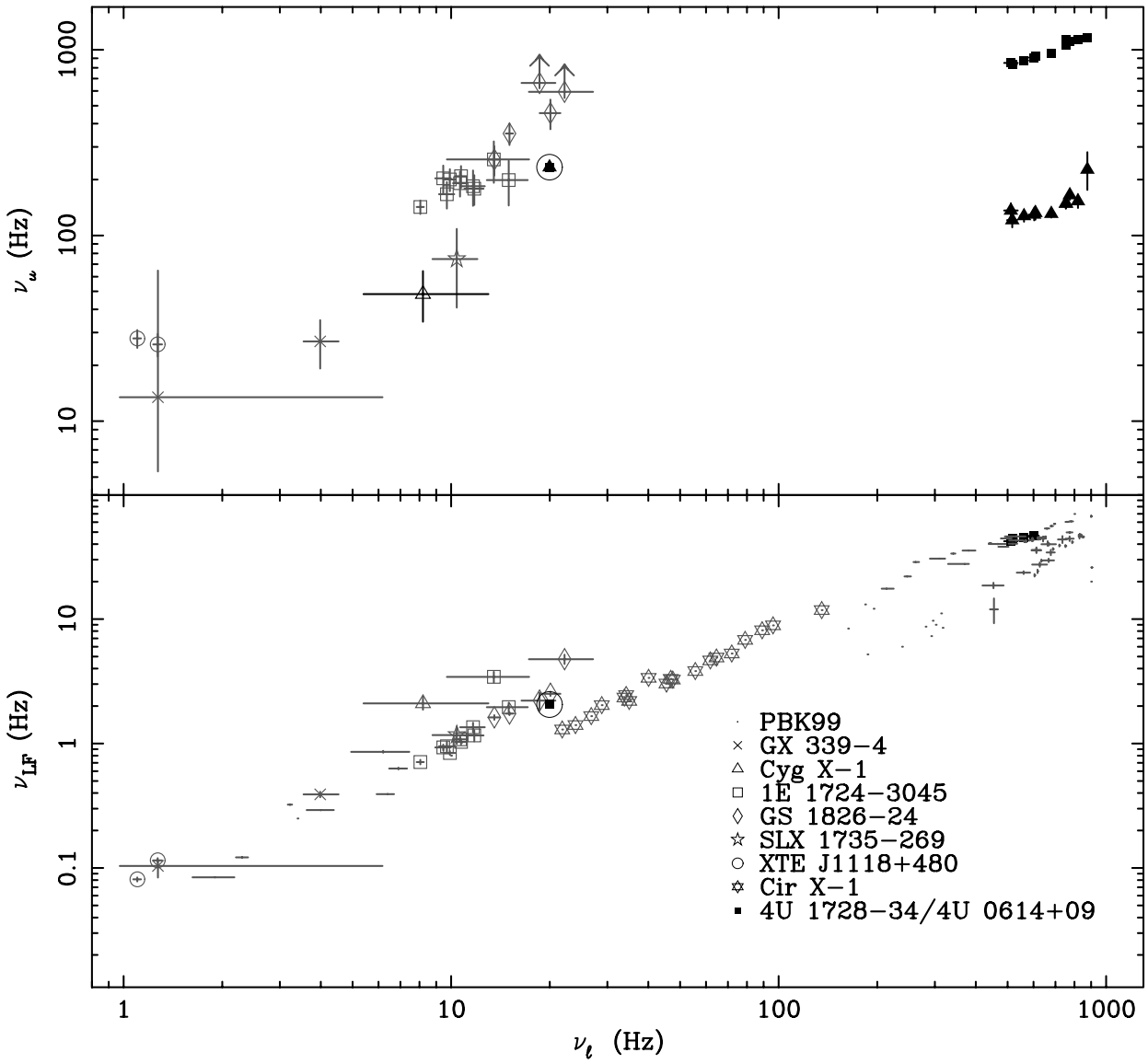

Fig. 8.— Our results compared to the relations shown in BPK01. The grey symbols represent the results on Shirey (1998), Nowak (2000) and BPK01, the black symbols our results of 4U 1728–34 and 4U 0614+09. The symbols representing the different sources are indicated in the plot. For 4U 1728–34 and 4U 0614+09 the squares in the top plot mark the upper kilohertz QPOs and the triangles the hectohertz Lorentzian. The arrows in the top panel indicate lower limits. The circled points are from interval 1 of 4U 0614+09, for which the Lorentzian at 233 Hz can be identified as either the upper kilohertz QPO or the hectohertz Lorentzian (see §3). Note that the differences between the lower panel and the corresponding plot in BPK01 (Figure 10) are due to the use of the characteristic frequency of the broad Lorentzian component as $\nu_{\rm LF}$ for both 1E 1724–3045 and GS 1826–24 instead of the narrow peak at similar centroid frequency (see §4).

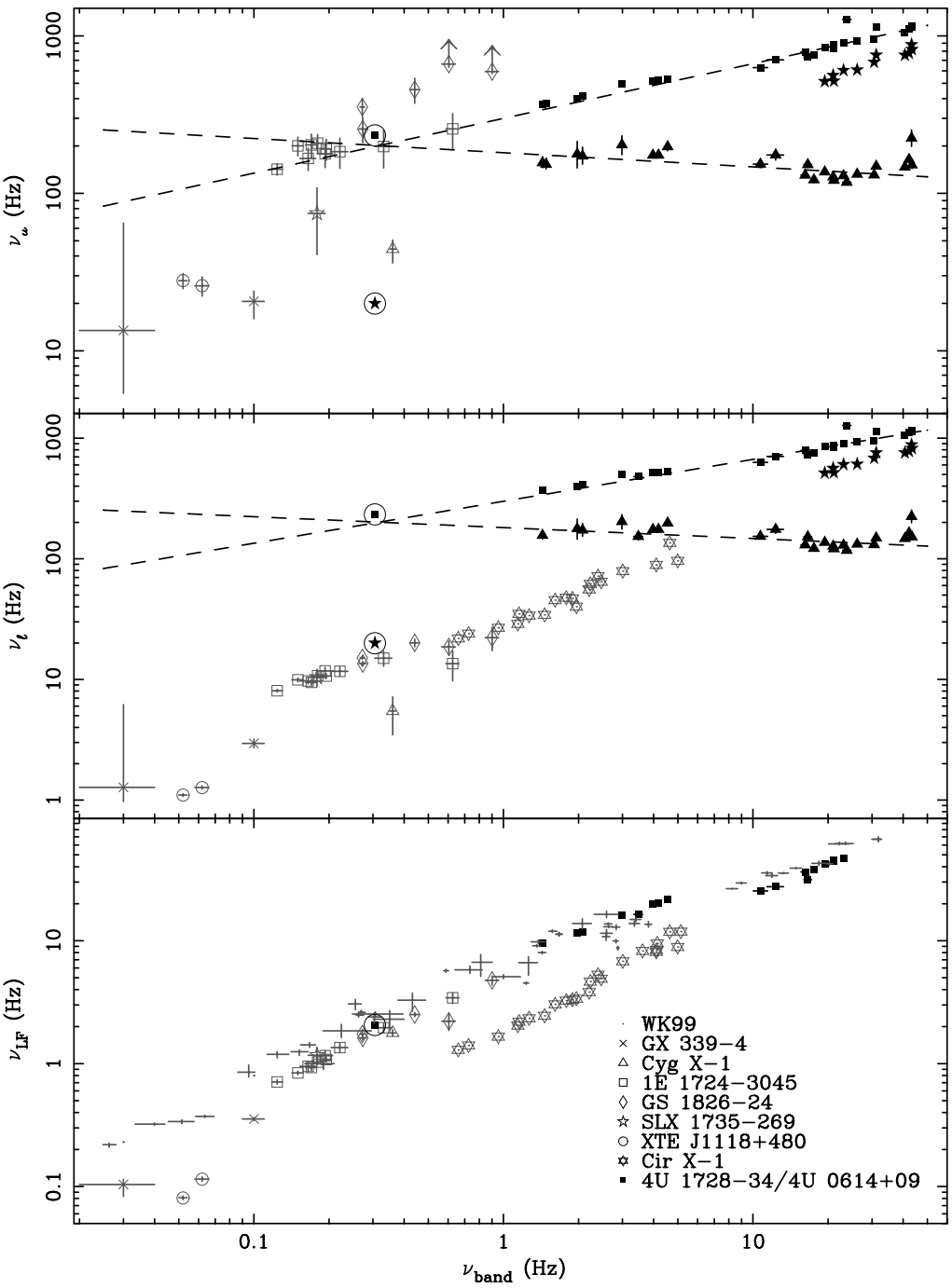

Fig. 9.— Comparison of the characteristic frequencies of the multi–Lorentzian fit to 4U 0614+09 and 4U 1728–34 with several other LMXBs. The grey symbols represent the results from Shirey (1998), Nowak (2000) and BPK01, the black symbols our results of 4U 1728–34 and 4U 0614+09. The symbols representing the different sources are indicated in the plot. For 4U 1728–34 and 4U 0614+09 the squares mark the upper kilohertz QPOs, the stars the lower kilohertz QPO, the triangles the hectohertz Lorentzian and the circles the low–frequency Lorentzian. For clarity the figure is split up in three panels. In the bottom panel we plot the characteristic frequency of the first Lorentzian versus the characteristic frequency of the band–limited noise (the WK99 relation). In the middle and top panels we plot the characteristic frequencies of the hectohertz Lorentzian and both kilohertz QPOs versus the characteristic frequency of the band–limited noise for 4U 1728–34 and 4U 0614+09. The dashed lines indicate extrapolated power–law fits (see §4) to the 4U 1728–34 and 4U 0614+09 points. In the midle panel we compare with the characteristic frequency of the second Lorentzian (ν_ℓ in PBK01) and in the top panel with the third Lorentzian (ν_u in PBK01) of Nowak (2000) and BPK01. The arrows in the top panel indicate lower limits. The circled points are from interval 1 of 4U 0614+09, for which the fourth Lorentzian can be identified as either the upper kilohertz QPO or the hectohertz Lorentzian (see §3).

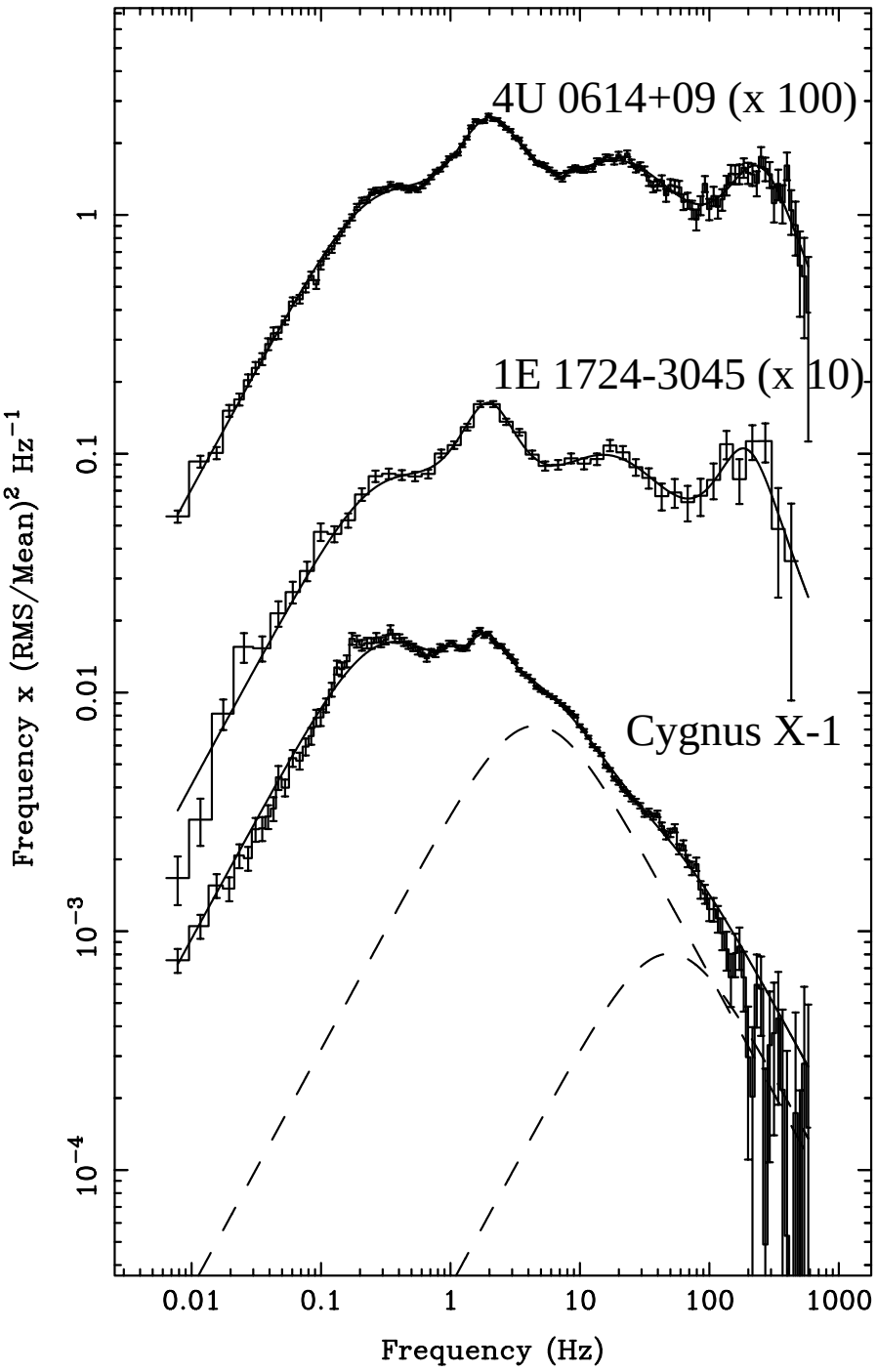

Fig. 10.— Power spectra and fit functions of 4U 0614+09, 1E 1724–3045 and Cyg X–1 all with a $\nu_{\rm band}$ of about 0.3 Hz. For clarity the power spectra of 4U 0614+09 and 1E 1724–3045 are multiplied with a constant as indicated in the plot. The dashed lines in the power spectra of Cyg X–1 show the individual two high frequency Lorentzians.